

Non-rotating and rotating neutron stars in the extended field theoretical model

Shashi K. Dhiman¹, Raj Kumar¹ and B. K. Agrawal²

¹*Department of Physics, H.P. University, Shimla - 171005, India.*

²*Saha Institute of Nuclear Physics, Kolkata - 700064, India.*

Abstract

We study the properties of non-rotating and rotating neutron stars for a new set of equations of state (EOSs) with different high density behaviour obtained using the extended field theoretical model. The high density behaviour for these EOSs are varied by varying the ω -meson self-coupling and hyperon-meson couplings in such a way that the quality of fit to the bulk nuclear observables, nuclear matter incompressibility coefficient and hyperon-nucleon potential depths remain practically unaffected. We find that the largest value for maximum mass for the non-rotating neutron star is $2.1M_{\odot}$. The radius for the neutron star with canonical mass is 12.8 – 14.1 km provided only those EOSs are considered for which maximum mass is larger than $1.6M_{\odot}$ as it is the lower bound on the maximum mass measured so far. Our results for the very recently discovered fastest rotating neutron star indicate that this star is supra massive with mass 1.7 – $2.7M_{\odot}$ and circumferential equatorial radius 12 – 19 km.

PACS numbers: 26.60.+c,91.60.Fe,97.10.Kc,97.10.Nf,97.10.Pg

I. INTRODUCTION

The knowledge of neutron star properties is necessary to probe the high density behaviour of the equation of state (EOS) for the baryonic matter in β -equilibrium. The EOS for the densities higher than $\rho_0 = 0.16 \text{ fm}^{-3}$ can be well constrained if radii for the neutron stars over a wide range of their masses are appropriately known. Even the accurate information on the maximum neutron star mass M_{max} and radius $R_{1.4}$ for the neutron star with canonical mass ($1.4M_{\odot}$) would narrow down the choices for the plausible EOSs to just a few. Till date, the neutron stars with masses only around $1.4M_{\odot}$ are accurately measured [1, 2, 3]. Recent measurement of mass of the pulsar PSR J0751+1807 imposes lower bounds on the maximum mass of the neutron star to be $1.6M_{\odot}$ and $1.9M_{\odot}$ with 95% and 68% confidence limits, respectively [4]. The increase in the lower bounds of the neutron star maximum mass could eliminate the family of EOSs in which exotica appear and substantial softening begins around 2 to 4 ρ_0 leading to appreciable reduction of the maximum mass. The available data on the neutron star radius have large uncertainties [5, 6, 7, 8, 9]. The main source of the uncertainties in the measurements of the neutron star radii are the unknown chemical composition of the atmosphere, inaccuracies in the star's distance and high magnetic field ($\sim 10^{12}$ G). Recent discovery of the binary neutron star system PSR J0737-3039A,B [2] with masses of the individual star being $1.338M_{\odot}$ and $1.249M_{\odot}$ have raised the hope for the possibility of measuring the moment of inertia due to the spin-orbit coupling effects [3]. It is expected that a reasonably accurate value for neutron star radius can be deduced from the moment of inertia measurements. Very recent discovery of the fastest rotating neutron star with rotational frequency of 1122 Hz observed in the X-ray transient XTE J1739-285 [10] has placed an additional constrained on the EOS at very high density [11].

Theoretically, the mass-radius relationship and compositions of the neutron stars are studied using various models which can be broadly grouped into (i) non-relativistic potential models [12], (ii) non-relativistic mean-field models [13, 14, 15, 16], (iii) field theoretical based relativistic mean-field models (FTRMF) [17, 18, 19] and (iv) Dirac-Brueckner-Hartree-Fock model [20, 21, 22, 23]. Each of these models can yield EOSs with different high density behaviour which is not yet well constrained. As a result, neutron star properties vary over a wide range even for the same model. In this work we shall mainly focus on the variations in the properties of the neutron stars obtained within the FTRMF models. The FTRMF

models predict the values of $M_{\max} = 1.2 - 3.0 M_{\odot}$ and $R_{1.4} = 10 - 16$ km for the non-rotating neutron stars [24, 25, 26]. The lower values of M_{\max} and $R_{1.4}$ correspond to the neutron stars composed of nucleons and hyperons in β -equilibrium, where as, the higher values of M_{\max} and $R_{1.4}$ correspond to the neutron stars with no hyperons. We would like to emphasize that not all the different parameterizations of the FTRMF model, employed to study the neutron star properties, are able to reproduce satisfactorily the basic properties of finite nuclei and nuclear matter at the saturation density. For instance, the value of the nuclear matter incompressibility coefficient which largely controls the low density behaviour of a EOS vary in between 200–360 MeV for different FTRMF models. Though, the value of nuclear matter incompressibility coefficient is very well constrained to 230 ± 10 MeV by the experimental data on the isoscalar giant monopole resonances in heavy nuclei [27, 28]. The variations in the neutron star properties resulting from the differences in the high density behaviour of the different EOSs can be appropriately studied only if the low density behaviour for each of these EOSs are constrained using the experimental data on the bulk properties of the finite nuclei and nuclear matter at the saturation density.

The extended FTRMF model [29, 30, 31] includes mixed and self-coupling terms for the σ , ω and ρ mesons. The ω -meson self-coupling term enables one to vary the high density behaviour of the EOS without affecting nuclear matter properties at the saturation density [24]. The mixed interaction terms involving ρ -mesons allow ones to significantly vary the density dependence of the symmetry energy coefficient [32, 33, 34] which plays crucial role in determining cooling mechanism of a neutron star [35]. Yet, such a versatile version of the FTRMF model is not fully explored to study the variations in the properties of the neutron stars resulting mainly from the uncertainties in the high density behaviour of EOS. In the present work we use the extended FTRMF models to obtain a new set of EOSs with different high density behaviour for the β -equilibrated matter composed of nucleons and hyperons. Each of these different EOSs correspond to different choices for the ω -meson self-coupling and hyperon-meson couplings which mainly affects the high density behaviour of a EOS. The remaining parameters of the model are calibrated using a set of experimental data on the total binding energy and charge rms radii for a few closed shell nuclei. In our calibrational procedure we also use the value of neutron-skin thickness for the ^{208}Pb nucleus as one of the data. Since, the neutron-skin thickness is only poorly known, we obtain different parameter sets for different neutron-skin thickness ranging from 0.16 – 0.28 fm. We further

restrict the parameters to yield a reasonable value for the nuclear matter incompressibility coefficient at the saturation density. We use our EOSs to study the mass-radius relationship and chemical compositions for non-rotating neutron stars. For the case of rotating neutron stars, we present our results for the Keplerian sequences and also investigate the variations of mass and circumferential equatorial radius for the very recently discovered fastest rotating neutron star.

In Sec. II we outline very briefly the Lagrangian density and corresponding energy density for the extended FTRMF model. In Sec. III we present our various parameterizations for different combinations of a ω -meson self-coupling, hyperon-meson couplings and neutron-skin thickness for the ^{208}Pb nucleus. In Sec. IV we present our results for the nuclear matter properties at the saturation density. In this section we also discuss about the quality of the fits to the finite nuclei for these parameterizations. In Sec. V we present our results for the properties of non rotating neutron stars. We also generate some rotating neutron star sequences for which the results are presented in Sec. VI. Finally our main conclusions are presented in Sec. VII.

II. EXTENDED FIELD THEORETICAL MODEL

The effective Lagrangian density for the FTRMF model generally describes the interactions of the baryons via the exchange of σ , ω and ρ mesons. The σ and the ω mesons are responsible for nuclear binding while ρ meson is required to obtain the correct value for the empirical symmetry energy. The cubic and quartic terms for the self-interaction of the σ -meson are often considered which significantly improves the value of the nuclear matter incompressibility. Nevertheless, the value of the nuclear matter incompressibility coefficient for these models are usually larger in comparison to their values extracted from the experimental data on the isoscalar giant monopole resonances. Moreover, the symmetry energy coefficient and its density dependence is also somewhat higher relative to the corresponding empirical estimates. One can easily overcome these issues in the extended FTRMF model which includes self and mixed interaction terms for σ , ω and ρ mesons upto the quartic order. In particular, mixed interaction terms involving rho-meson field enables one to vary the density dependence of the symmetry energy coefficient and the neutron skin thickness in heavy nuclei over a wide range without affecting the other properties of finite nuclei [33, 34].

The contribution from the self interaction of ω -mesons plays important role in varying the high density behaviour of the EOS and also prevents instabilities in the calculation of the EOS [24, 36]. On the other hand expectation value of the ρ -meson field is order of magnitude smaller than that for the ω -meson field [31]. Thus, inclusion of the ρ -meson self interaction can affect the properties of the finite nuclei and neutron stars only very marginally [24].

The Lagrangian density for the extended FTRMF model can be written as,

$$\mathcal{L} = \mathcal{L}_{\mathcal{BM}} + \mathcal{L}_\sigma + \mathcal{L}_\omega + \mathcal{L}_\rho + \mathcal{L}_{\sigma\omega\rho} + \mathcal{L}_{em} + \mathcal{L}_{e\mu} + L_{YY}. \quad (1)$$

Where the baryonic and mesonic Lagrangian $\mathcal{L}_{\mathcal{BM}}$ can be written,

$$\mathcal{L}_{\mathcal{BM}} = \sum_B \bar{\Psi}_B [i\gamma^\mu \partial_\mu - (M_B - g_{\sigma B}\sigma) - (g_{\omega B}\gamma^\mu \omega_\mu + \frac{1}{2}g_{\rho B}\gamma^\mu \tau_B \cdot \rho_\mu)] \Psi_B. \quad (2)$$

Here, the sum is taken over the complete baryon octet which consists of nucleons, Λ , Σ and Ξ hyperons. For the calculation of finite nuclei properties only neutron and proton has been considered. τ_B are the isospin matrices. The Lagrangian describing self interactions for σ , ω , and ρ mesons can be written as,

$$\mathcal{L}_\sigma = \frac{1}{2}(\partial_\mu \sigma \partial^\mu \sigma - m_\sigma^2 \sigma^2) - \frac{\bar{\kappa}}{3!} g_{\sigma N}^3 \sigma^3 - \frac{\bar{\lambda}}{4!} g_{\sigma N}^4 \sigma^4, \quad (3)$$

$$\mathcal{L}_\omega = -\frac{1}{4} \omega_{\mu\nu} \omega^{\mu\nu} + \frac{1}{2} m_\omega^2 \omega_\mu \omega^\mu + \frac{1}{4!} \zeta g_{\omega N}^4 (\omega_\mu \omega^\mu)^2, \quad (4)$$

$$\mathcal{L}_\rho = -\frac{1}{4} \rho_{\mu\nu} \rho^{\mu\nu} + \frac{1}{2} m_\rho^2 \rho_\mu \rho^\mu + \frac{1}{4!} \xi g_{\rho N}^4 (\rho_\mu \rho^\mu)^2. \quad (5)$$

The $\omega^{\mu\nu}$, $\rho^{\mu\nu}$ are field tensors corresponding to the ω and ρ mesons, and can be defined as $\omega^{\mu\nu} = \partial^\mu \omega^\nu - \partial^\nu \omega^\mu$ and $\rho^{\mu\nu} = \partial^\mu \rho^\nu - \partial^\nu \rho^\mu$. The mixed interactions of σ , ω , and ρ mesons $\mathcal{L}_{\sigma\omega\rho}$ can be written as,

$$\begin{aligned} \mathcal{L}_{\sigma\omega\rho} &= g_{\sigma N} g_{\omega N}^2 \sigma \omega_\mu \omega^\mu \left(\bar{\alpha}_1 + \frac{1}{2} \bar{\alpha}_1' \sigma \right) + g_{\sigma N} g_{\rho N}^2 \sigma \rho_\mu \rho^\mu \left(\bar{\alpha}_2 + \frac{1}{2} \bar{\alpha}_2' \sigma \right) \\ &+ \frac{1}{2} \bar{\alpha}_3' g_{\omega N}^2 g_{\rho N}^2 \omega_\mu \omega^\mu \rho_\mu \rho^\mu \end{aligned} \quad (6)$$

The \mathcal{L}_{em} is Lagrangian for electromagnetic interactions and can be expressed as,

$$\mathcal{L}_{em} = -\frac{1}{4} F_{\mu\nu} F^{\mu\nu} - \sum_B e \bar{\Psi}_B \gamma_\mu \frac{1 + \tau_{3B}}{2} A_\mu \Psi_B, \quad (7)$$

where, $F^{\mu\nu} = \partial^\mu A^\nu - \partial^\nu A^\mu$. The hyperon-hyperon interaction has been included by introducing two additional mesonic fields (σ^* and ϕ) and the corresponding Lagrangian \mathcal{L}_{YY}

($Y = \Lambda, \Sigma$, and Ξ) can be written as,

$$\begin{aligned} \mathcal{L}_{YY} &= \sum_Y \bar{\Psi}_Y (g_{\sigma^* Y} \sigma^* - g_{\phi Y} \gamma^\mu \phi_\mu) \Psi_Y \\ &+ \frac{1}{2} (\partial_\nu \sigma^* \partial^\nu \sigma^* - m_{\sigma^*}^2 \sigma^{*2}) - \frac{1}{4} S_{\mu\nu} S^{\mu\nu} + \frac{1}{2} m_\phi^2 \phi_\mu \phi^\mu. \end{aligned} \quad (8)$$

The charge neutral neutron star matter also includes leptons such as e^- and μ^- in addition to neutrons, proton, and hyperons at the high densities. The leptonic contributions to the total Lagrangian density can be written as,

$$\mathcal{L}_{e\mu} = \sum_{\ell=e,\mu} \bar{\Psi}_\ell (i\gamma^\mu \partial_\mu - M_\ell) \Psi_\ell. \quad (9)$$

The equation of motion for baryons, mesons and photons can be derived from the Lagrangian density defined in Eq.(1). The equation of motion for baryons can be given as,

$$\begin{aligned} &\left[\gamma^\mu \left(i\partial_\mu - g_{\omega B} \omega_\mu - \frac{1}{2} g_{\rho B} \tau_B \cdot \rho_\mu - e \frac{1 + \tau_{3B}}{2} A_\mu - g_{\phi B} \phi^\mu \right) - \right. \\ &\left. (M_B + g_{\sigma B} \sigma + g_{\sigma^* B} \sigma^*) \right] \Psi_B = \epsilon_B \Psi_B. \end{aligned} \quad (10)$$

The Euler-Lagrange equations for the ground state expectation values of the mesons fields are:

$$\begin{aligned} (-\Delta + m_\sigma^2) \sigma &= \sum_B g_{\sigma B} \rho_{sB} - \frac{\bar{K}}{2} g_{\sigma N}^3 \sigma^2 - \frac{\bar{\lambda}}{6} g_{\sigma N}^4 \sigma^3 + \bar{\alpha}_1 g_{\sigma N} g_{\omega N}^2 \omega^2 \\ &+ \bar{\alpha}'_1 g_{\sigma N}^2 g_{\omega N}^2 \sigma \omega^2 + \bar{\alpha}_2 g_{\sigma N} g_{\rho B}^2 \rho^2 + \bar{\alpha}'_2 g_{\sigma N}^2 g_{\rho N}^2 \sigma \rho^2, \end{aligned} \quad (11)$$

$$\begin{aligned} (-\Delta + m_\omega^2) \omega &= \sum_B g_{\omega B} \rho_B - \frac{\zeta}{6} g_{\omega N}^4 \omega^3 - 2\bar{\alpha}_1 g_{\sigma N} g_{\omega N}^2 \sigma \omega - \bar{\alpha}'_1 g_{\sigma N}^2 g_{\omega N}^2 \sigma^2 \omega \\ &- \bar{\alpha}'_3 g_{\omega N}^2 g_{\rho N}^2 \omega \rho^2, \end{aligned} \quad (12)$$

$$\begin{aligned} (-\Delta + m_\rho^2) \rho &= \sum_B g_{\rho B} \tau_{3B} \rho_B - \frac{\xi}{6} g_{\rho N}^4 \rho^3 - 2\bar{\alpha}_2 g_{\sigma N} g_{\rho N}^2 \sigma \rho - \bar{\alpha}'_2 g_{\sigma N}^2 g_{\rho N}^2 \sigma^2 \rho \\ &- \bar{\alpha}'_3 g_{\omega N}^2 g_{\rho N}^2 \omega^2 \rho, \end{aligned} \quad (13)$$

$$(-\Delta + m_{\sigma^*}^2) \sigma^* = \sum_B g_{\sigma^* B} \rho_{sB}, \quad (14)$$

$$(-\Delta + m_\phi^2) \phi = \sum_B g_{\phi B} \rho_B, \quad (15)$$

$$-\Delta A_0 = e \rho_p. \quad (16)$$

where the baryon density ρ_B , scalar density ρ_{sB} and charge density ρ_p are, respectively,

$$\rho_B = \langle \bar{\Psi}_B \gamma^0 \Psi_B \rangle = \frac{\gamma k_B^3}{6\pi^2}, \quad (17)$$

$$\rho_{sB} = \langle \bar{\Psi}_B \Psi_B \rangle = \frac{\gamma}{(2\pi)^3} \int_0^{k_B} d^3k \frac{M_B^*}{\sqrt{k^2 + M_B^{*2}}}, \quad (18)$$

$$\rho_p = \left\langle \bar{\Psi}_B \gamma^0 \frac{1 + \tau_{3B}}{2} \Psi_B \right\rangle. \quad (19)$$

Where, γ is the spin degeneracy. The $M_B^* = M_B - g_{\sigma B} \sigma - g_{\sigma^* B} \sigma^*$ is the effective mass of the baryon species B, k_B is its Fermi momentum and τ_{3B} denotes the isospin projections of baryon B.

The energy density of the uniform matter in the extended FTRMF models is given by

$$\begin{aligned} \mathcal{E} = & \sum_{j=B,\ell} \frac{1}{\pi^2} \int_0^{k_j} k^2 \sqrt{k^2 + M_j^{*2}} dk + \sum_B g_{\omega B} \omega \rho_B + \sum_B g_{\rho B} \tau_{3B} \rho + \frac{1}{2} m_\sigma^2 \sigma^2 \\ & + \frac{\bar{\kappa}}{6} g_{\sigma N}^3 \sigma^3 + \frac{\bar{\lambda}}{24} g_{\sigma N}^4 \sigma^4 - \frac{\zeta}{24} g_{\omega N}^4 \omega^4 - \frac{\xi}{24} g_{\rho N}^4 \rho^4 - \frac{1}{2} m_\omega^2 \omega^2 - \frac{1}{2} m_\rho^2 \rho^2 \\ & - \bar{\alpha}_1 g_{\sigma N} g_{\omega N}^2 \sigma \omega^2 - \frac{1}{2} \bar{\alpha}'_1 g_{\sigma N}^2 g_{\omega N}^2 \sigma^2 \omega^2 - \bar{\alpha}_2 g_{\sigma N} g_{\rho N}^2 \sigma \rho^2 - \frac{1}{2} \bar{\alpha}'_2 g_{\sigma N}^2 g_{\rho N}^2 \sigma^2 \rho^2 \\ & - \frac{1}{2} \bar{\alpha}'_3 g_{\omega N}^2 g_{\rho N}^2 \omega^2 \rho^2 + \frac{1}{2} m_{\sigma^*}^2 \sigma^{*2} + \sum_B g_{\phi B} \phi \rho_B - \frac{1}{2} m_\phi^2 \phi^2. \end{aligned} \quad (20)$$

The pressure of the uniform matter is given by

$$\begin{aligned} P = & \sum_{j=B,\ell} \frac{1}{3\pi^2} \int_0^{k_j} \frac{k^4 dk}{\sqrt{k^2 + M_j^{*2}}} - \frac{1}{2} m_\sigma^2 \sigma^2 - \frac{\bar{\kappa}}{6} g_{\sigma N}^3 \sigma^3 - \frac{\bar{\lambda}}{24} g_{\sigma N}^4 \sigma^4 \\ & + \frac{\zeta}{24} g_{\omega N}^4 \omega^4 + \frac{\xi}{24} g_{\rho N}^4 \rho^4 + \frac{1}{2} m_\omega^2 \omega^2 + \frac{1}{2} m_\rho^2 \rho^2 + \bar{\alpha}_1 g_{\sigma N} g_{\omega N}^2 \sigma \omega^2 \\ & + \frac{1}{2} \bar{\alpha}'_1 g_{\sigma N}^2 g_{\omega N}^2 \sigma^2 \omega^2 + \bar{\alpha}_2 g_{\sigma N} g_{\rho N}^2 \sigma \rho^2 + \frac{1}{2} \bar{\alpha}'_2 g_{\sigma N}^2 g_{\rho N}^2 \sigma^2 \rho^2 \\ & + \frac{1}{2} \bar{\alpha}'_3 g_{\omega N}^2 g_{\rho N}^2 \omega^2 \rho^2 - \frac{1}{2} m_{\sigma^*}^2 \sigma^{*2} + \frac{1}{2} m_\phi^2 \phi^2. \end{aligned} \quad (21)$$

III. PARAMETERIZATIONS OF THE EXTENDED FTRMF MODEL

In this section we consider various parameterizations of the extended FTRMF model. The different parameter sets are obtained using different values for the ω -meson self-coupling ζ , hyperon-meson couplings g_{iY} ($i = \sigma, \omega, \rho, \sigma^*$ and ϕ mesons) and neutron-skin thickness Δr for the ^{208}Pb nucleus. The parameter ζ mainly affects the high density behaviour of the EOS

and can not be well constrained by the properties of the finite nuclei. The different sets of g_{iY} can be obtained to yield different EOSs for the dense matter without affecting the resulting potential depth for hyperons in the nuclear matter at the saturation density. The value of Δr for a single heavy nucleus like ^{208}Pb which can constrain the linear density dependence of the symmetry energy is only poorly known. The different choices for the ζ , g_{iY} and Δr are so made that they span entire range of values as often used in the literature. We must point out that the contributions from the ρ -meson self-coupling are ignored, because, their effects are found to be only marginal even for the pure neutron matter at very high densities [24].

Towards our parameterizational procedure we first set hyperon-meson couplings $g_{iY} = 0$ in Eqs. (2,8). Then the remaining coupling parameters appearing in Eqs. (2 - 6) are determined by fitting the FTRMF results to the experimental data for the total binding energies and charge rms radii for many closed shell normal and exotic nuclei. We consider total binding energies for $^{16,24}\text{O}$, $^{40,48}\text{Ca}$, $^{56,78}\text{Ni}$, ^{88}Sr , ^{90}Zr , $^{100,116,132}\text{Sn}$ and ^{208}Pb nuclei, charge rms radii for ^{16}O , $^{40,48}\text{Ca}$, ^{56}Ni , ^{88}Sr , ^{90}Zr , ^{116}Sn and ^{208}Pb nuclei. In addition, we also fit the value of neutron-skin thickness for ^{208}Pb nucleus. Recently extracted value of neutron-skin thickness for ^{208}Pb nucleus from the isospin diffusion data lie within 0.16 – 0.24 fm indicating large uncertainties [37]. We generate twenty one different parameter sets using different combinations of ζ and Δr . The value of ζ is taken to be 0.0, 0.03 and 0.06 and for the Δr we use 0.16, 0.18, ..., 0.28 fm. The best fit parameters are obtained by minimizing the χ^2 function given as,

$$\chi^2 = \frac{1}{N_d - N_p} \sum_{i=1}^{N_d} \left(\frac{\mathcal{O}_i^{exp} - \mathcal{O}_i^{th}}{\delta_i} \right)^2 \quad (22)$$

where, N_d is the number of experimental data points and N_p the number of parameters to be fitted. The δ_i stands for theoretical error and \mathcal{O}_i^{exp} and \mathcal{O}_i^{th} are the experimental and the corresponding theoretical values, respectively, for a given observable. Since, the \mathcal{O}_i^{th} in Eq.(22) is calculated using the FTRMF model, the value of χ^2 depends on the values of the parameters appearing in Eq. (2 - 6). The theoretical error δ_i in Eq.(22) are taken to be 1.0 MeV for the total binding energies, 0.02 fm for the charge rms radii and 0.005 fm for the neutron-skin thickness. The best fit parameters for a given set of values of \mathcal{O}_i^{exp} and δ_i are searched using the simulated annealing method [38, 39]. In our earlier work [39] we have obtained the parameter sets for $\zeta = 0.0, 0.03$ and 0.06 with $\Delta r = 0.18$ fm. Here too we

follow the same strategy to obtain the parameter set for a given combination of Δr and ζ . In Tables I, II and III we list the values of parameters for all the sets presently generated.

We now determine the values of the hyperon-meson coupling parameters g_{iY} . These couplings can be expressed in terms of the nucleon-meson couplings using SU(6) model as,

$$\begin{aligned}
\frac{1}{3}g_{\sigma N} &= \frac{1}{2}g_{\sigma\Lambda} = \frac{1}{2}g_{\sigma\Sigma} = g_{\sigma\Xi}, \\
\frac{1}{3}g_{\omega N} &= \frac{1}{2}g_{\omega\Lambda} = \frac{1}{2}g_{\omega\Sigma} = g_{\omega\Xi}, \\
g_{\rho N} &= g_{\rho\Sigma} = 2g_{\rho\Xi}, \quad g_{\rho\Lambda} = 0, \\
2g_{\sigma^*\Lambda} &= 2g_{\sigma^*\Sigma} = g_{\sigma^*\Xi} = \frac{2\sqrt{2}}{3}g_{\omega N}, \quad g_{\sigma^*N} = 0, \\
2g_{\phi\Lambda} &= 2g_{\phi\Sigma} = g_{\phi\Xi} = \frac{2\sqrt{2}}{3}g_{\omega N}, \quad g_{\phi N} = 0.
\end{aligned} \tag{23}$$

The neutron star properties are quite sensitive to the values of $g_{\sigma Y}$ and $g_{\omega Y}$. Where as neutron star properties do not get significantly affected even if the values of $g_{\sigma^* Y}$ is varied over a reasonable range for a fixed value of $g_{\phi Y}$ [40]. For $g_{\rho Y}$, $g_{\sigma^* Y}$ and $g_{\phi Y}$ we use the values as given by Eq. (23). The values of $g_{\sigma Y}$ and $g_{\omega Y}$ are determined using the expressions for the hyperon-nucleon potential. The potential depth for a given hyperon species in the nuclear matter at the saturation density (ρ_{sat}) is given as,

$$U_Y^{(N)}(\rho_{sat}) = -g_{\sigma Y}\sigma(\rho_{sat}) + g_{\omega Y}\omega(\rho_{sat}). \tag{24}$$

The values of $U_Y^{(N)}$ chosen are as follows [41],

$$U_{\Lambda}^{(N)} = -28 \text{ MeV}, \quad U_{\Sigma}^{(N)} = +30 \text{ MeV} \quad \text{and} \quad U_{\Xi}^{(N)} = -18 \text{ MeV}. \tag{25}$$

Normally, $g_{\sigma Y}$ is determined for a given value of $U_Y^{(N)}(\rho_{sat})$ with $g_{\omega Y}$ taken from SU(6) model. For the sake of convenience we define,

$$X_{mY} = \begin{cases} \left(\frac{g_{mY}}{g_{mN}} \right) & \text{for } \Lambda \text{ and } \Sigma \text{ hyperons} \\ 2 \left(\frac{g_{mY}}{g_{mN}} \right) & \text{for } \Xi \text{ hyperons,} \end{cases} \tag{26}$$

where, m stands for σ and ω mesons. In the present work we vary $X_{\omega Y}$ from 0.5 – 0.8 [42]. In Fig. 1 we display the variations of $X_{\sigma Y}$ as a function of $X_{\omega Y}$ obtained using the parameter set corresponding to $\zeta = 0.03$ and $\Delta r = 0.22$ fm. The values of $X_{\sigma Y}$ are for all other combinations of ζ and Δr are very much the same as depicted in Fig. 1. This is

due to the fact that the properties of symmetric nuclear matter, like, binding energy per nucleon B/A , nuclear matter incompressibility coefficient K , effective nucleon mass M_N^* at the saturation density are very much similar for all the parameterizations considered in the present work.

IV. NUCLEAR MATTER AND FINITE NUCLEI

The various properties associated with the nuclear matter are obtained using parameter sets of Tables I, II and III. The values of B/A , K , M_N^* and ρ_{sat} for all these parameter sets lie in a narrow range. We find that $B/A = 16.11 \pm 0.04$ MeV, $K = 230.24 \pm 9.80$ MeV, $M_N^*/M_N = 0.605 \pm 0.004$ and $\rho_{sat} = 0.148 \pm 0.003$ fm⁻³. The values of the symmetry energy coefficient J and its linear density dependence,

$$L = 3\rho \left. \frac{dJ}{d\rho} \right|_{\rho_{sat}} \quad (27)$$

are strongly correlated with the Δr for the ²⁰⁸Pb nucleus used in the fit. In Fig. 2 we display the variations of J and L calculated at saturation density as a function of Δr . The values of L lie in the range of 80 ± 20 MeV for Δr varying in between 0.16 to 0.28 fm which is in reasonable agreement with the recent predictions based on the isospin diffusion data [37].

The relative errors in the total binding energy and charge rms radius for the nuclei included in the fits are more or less the same as we have obtained in our earlier work [39]. So, we do not wish to present here the detailed results. It might be sufficient for the present purpose to display the results for the rms errors for the total binding energies and charge rms radii obtained for our newly generated parameter sets. In Fig. 3 we plot the rms errors for the total binding energies and charge radii as a function of Δr . It is quite clear from this figure that rms error show hardly any variations implying that all the parameter sets generated in the present work fit the finite nuclear properties equally well. In fact, if we do not consider the parameterizations with $\zeta = 0.0$ and $\Delta r = 0.26$ or 0.28 fm, the rms errors on the total binding energy are 1.5 - 1.8 MeV which is comparable with one obtained using NL3 parameterizations as most commonly used [43]. The rms error of charge radii for the nuclei considered in the fit lie within the 0.025 – 0.040 fm.

V. NON-ROTATING NEUTRON STARS

In this section we present our results for the properties of the non-rotating neutron stars for a set of EOSs obtained using different parameterizations for the extended FTRMF model. Each of these parameterizations corresponds to different combinations of neutron-skin thickness Δr in ^{208}Pb nucleus, the ω -meson self-coupling ζ and hyperon-meson couplings $X_{\omega Y}$ as described in Sec. III. The values of Δr , ζ and $X_{\omega Y}$ are so varied that they span the entire range of values as often encountered in the literature. The variations in ζ and $X_{\omega Y}$ affect the high density behaviour of the EOS, whereas, the density dependence of the symmetry energy coefficient is strongly correlated with Δr . It is therefore natural to expect that the variations in Δr , ζ and $X_{\omega Y}$ can affect significantly the neutron star properties. The parameters of FTRMF model are so calibrated that the quality of fit to finite nuclei, the properties of nuclear matter at saturation density and hyperon-nucleon potentials are almost the same for each of the parameterizations. Thus, these parameterizations provide the right starting point to study the actual variations in the properties of neutron star resulting from the uncertainties in the EOS of dense matter.

The properties of non-rotating neutron stars are obtained by integrating the Tolman-Oppenheimer-Volkoff (TOV) equations [44]. To solve the TOV equations we use the EOS for the matter consisting of nucleons, hyperons and leptons. The composition of matter at fixed total baryon density,

$$\rho = \sum_B \rho_B, \quad (28)$$

are so determined that charge neutrality condition,

$$\sum_B q_B \rho_B + \sum_\ell q_\ell \rho_\ell = 0, \quad (29)$$

and chemical equilibrium conditions,

$$\mu_B = \mu_n - q_B \mu_e \quad (30)$$

$$\mu_\mu = \mu_e \quad (31)$$

are satisfied. In Eqs. (29-31) q and μ are the charge and chemical potential for various baryons and leptons considered in our calculations. For densities higher than $0.5\rho_0$, the baryonic part of EOS is evaluated within the FTRMF model. Whereas, the contributions of the electrons and muons to the EOS are evaluated within the Fermi gas approximation. At

densities lower than $0.5\rho_0$ down to $0.4 \times 10^{-10}\rho_0$ we use the EOS of Baym-Pethick-Sutherland (BPS) [45].

In Fig. 4 we plot the EOS for the pure neutron matter and symmetric nuclear matter as a function of number density for the selected combinations of ζ and Δr . We see that the EOS for $\zeta = 0.0$ is the most stiffest, and as ζ increases the EOS becomes softer. The softening of EOS with ζ is more pronounced at higher densities. In Fig. 5 we plot our results for the neutron and electron chemical potentials as a function of baryon density obtained for the EOSs corresponding to the moderate values of Δr and $X_{\omega Y}$. The chemical potentials for other particles can be evaluated using Eqs. (30) and (31). The change in slope for neutron chemical potential vs. baryon density is associated with appearance of hyperons. The decrease in μ_e for $\rho \geq 2\rho_0$ is accompanied by the appearance of the Ξ^- hyperons. The maximum values of μ_e is less than half of the bare mass for kaons which indicate that the presence of hyperons inhibits the kaon condensation.

Let us now consider various neutron star properties resulting from the EOSs for the two different parameter sets referred hereafter as LY and UY. These parameter sets are obtained using different combinations of Δr , ζ and $X_{\omega Y}$. The parameters of LY set are obtained with $\Delta r = 0.16$ fm, $\zeta = 0.06$ and $X_{\omega Y} = 0.5$. Whereas, UY parameterization is obtained with $\Delta r = 0.28$ fm, $\zeta = 0.0$ and $X_{\omega Y} = 0.8$. Among all the parameterizations as obtained in Sec. III, LY and UY yield the softest and the stiffest EOSs, respectively. Thus, maximum variations in the neutron star properties can be studied using the EOSs obtained for LY and UY parameter sets. For the comparison, we also present our results for the L0 and U0 parameter sets similar to LY and UY parameterizations, but, with no hyperons. In Fig. 6 we present our results for mass-radius relationship for LY, UY, L0 and U0 parameterizations. The region bounded by $R \leq 3GM/c^2$ is excluded by the causality limit [46]. The line labeled by $\Delta I/I = 0.014$ is radius limit estimated by Vela pulsar glitches [47]. The rotation constraint as indicated in Fig. 6 is obtained using [48],

$$\nu_k = 1833\eta \left(\frac{M}{M_\odot}\right)^{1/2} \left(\frac{10\text{km}}{R}\right)^{3/2} \text{ Hz} \quad (32)$$

with $\eta = 0.57$ and $\nu_k = 1122$ Hz which corresponds to the frequency for the fastest rotating neutron star present in the recently observed X-ray transient XTE J1739-285 [10]. The renormalization factor η account for the effects due to deformation and gravity. We also

calculate the variations in the radiation radius,

$$R_\infty = \frac{R}{\sqrt{1 - \frac{2GM}{Rc^2}}} \quad (33)$$

for the neutron star with the canonical mass $1.4M_\odot$. It can be verified by using the results for the LY and UY cases presented in Fig. 6 that R_∞ lies in the range of 14.2 – 16.8 km. Similarly, without the inclusion of hyperons, the values of R_∞ vary in the range of 15.3 – 16.8 km. In Tables IV and V we collect few important bulk properties for the non-rotating neutron stars with maximum and canonical masses. We see that the values of M_{\max} with the inclusion of hyperons varies between $1.4 - 2.1M_\odot$. Once the contributions from the hyperons are ignored M_{\max} varies between $1.7 - 2.4M_\odot$. The values of $R_{1.4}$ varies from 11.3 – 14.1 km and 12.5 – 14.1 km depending on whether the hyperonic contributions are included or not. Thus, combining our results for the neutron stars with and without hyperons we find that the values of M_{\max} and $R_{1.4}$ obtained within the FTRMF model can vary about $1M_\odot$ and 3 km, respectively. These variations are almost half of the ones obtained earlier using FTRMF model in which bulk nuclear observables and nuclear matter incompressibility were not fitted appropriately. The values of redshift given in the Tables IV and V are obtained for the ratio M/R as,

$$Z = \frac{1}{\sqrt{1 - \frac{2GM}{Rc^2}}} - 1. \quad (34)$$

Our results for the values of redshift for the neutron star with canonical mass are 0.22 ± 0.03 . It is also interesting to note that $Z \geq 0.35$ only for the stars with masses $1.7M_\odot$ or larger.

In Fig. 7 we have plotted the threshold densities for various hyperon species. In the same figure we also show the values of central densities for the neutron stars with canonical mass and maximum mass. The threshold density is lowest for the Λ hyperons. It is interesting to note that for the UY case the threshold density for the Λ hyperons is almost equal to the central density for the neutron star with the canonical mass. This implies that the properties of the neutron star with the canonical mass do not get affected by the hyperons for the UY parameterization. This is the reason that our results for the mass and radius for U0 and UY parameterizations are very much similar for the neutron stars with masses upto $1.6M_\odot$ as can be seen from Fig. 6. The Σ^+ and Σ^0 hyperons do not appear in density range relevant for the present study. However, for the TM1 parameterization of the FTRMF model one

finds that all kinds of hyperons appear well below $7\rho_0$ [49, 50]. This seems to be due to large value of nuclear matter incompressibility coefficient ($K = 281$ MeV) associated with the TM1 parameter set. In other words, not only the variations in the properties of the neutron stars reduces but also the chemical compositions for these stars can become different if the parameters of the FTRMF models are calibrated appropriately. In Fig. 8 we plot the particle fractions as a function of radial coordinate. These fractions are calculated for the neutron stars with $M_{\max} = 1.4M_{\odot}$ and $2.1M_{\odot}$ corresponding to the LY (upper panel) and UY (lower panel) parameterizations, respectively. The neutron fractions in Fig. 8 are plotted after dividing them by a factor of three. We see that the compositions of the neutron stars shown in the upper and lower panels are not the same. For the case of LY parameterizations, Ξ^- and Σ^- hyperons appear more or less simultaneously. For the UY case, Ξ^0 hyperons appear instead of Σ^- hyperons. It is noteworthy that for the case with UY parameterization the hyperons are the dominant particles at the interior ($r < 4$ km) of the neutron star leading to complete deleptonization. We see from Fig. 8 that the proton fractions for both the cases are greater than the critical value ($\sim 15\%$) for the Direct Urca process to occur [35].

We now consider our results for neutron star properties at the canonical and maximum masses for the set of EOSs obtained using all the different parameterizations as given in Sec. III. These different parameterizations correspond to the different combinations of the Δr , ζ and $X_{\omega Y}$. The values of Δr , ζ and $X_{\omega Y}$ vary in the range $0.16 - 0.28$ fm, $0.0 - 0.06$ and $0.5 - 0.8$, respectively. The knowledge of M_{\max} and ($R_{1.4}$) or moment of inertia ($\mathcal{I}_{1.4}$) for neutron star with canonical mass are very important in order to understand the behaviour of the EOS over the wide range of density well above ρ_0 . The discovery of the pulsars PSR J0737-3039A,B and PSR J0751+1807 have raised hope for availability of more accurate information about these quantities in near future. The M_{\max} probes densest segment of the EOS. Whereas, $R_{1.4}$ or $\mathcal{I}_{1.4}$ probes relatively lower density region of EOS. It is not possible to say a priori whether or not M_{\max} is correlated to the properties of neutron star with $1.4M_{\odot}$. Earlier studies using FTRMF models indicate some correlations between M_{\max} and $R_{1.4}$ [19]. Another study carried out for 25 EOSs taken from different models show hardly any correlations between M_{\max} and $\mathcal{I}_{1.34}$ [51]. In Fig. 9 we plot the variations of radius and the redshift for the neutron star with the canonical mass as a function of M_{\max} . We see that M_{\max} varies between $1.4 - 2.1M_{\odot}$ and $R_{1.4}$ varies between $11.3 - 14.1$ km. The vertical line at $M_{\max} = 1.6M_{\odot}$ corresponds to the mass of the PSR J0751+1807 measured with 95%

confidence limit. If only those EOSs are considered for which $M_{\max} \geq 1.6M_{\odot}$ then the value of $R_{1.4}$ would lie in the range of 12.8 – 14.1 km. This result is in reasonable agreement with $R_{1.4} = 14.8_{-1.6}^{+1.8}$ km as deduced very recently by adequately fitting the high quality X-ray spectrum from the neutron star X7 in the globular cluster 47 Tucanae [52]. We also note strong correlations of M_{\max} with $R_{1.4}$ and $Z_{1.4}$. For a given value of M_{\max} , the spread in the values of $R_{1.4}$ is 0.7 ± 0.1 km. Only for the $M_{\max} \sim 1.4M_{\odot}$ we find that spread in the values of $R_{1.4}$ is ~ 0.3 km. To understand it better, we list in Table VI the values of M_{\max} and $R_{1.4}$ obtained for the sets of EOSs corresponding to the selected combinations of Δr , ζ and $X_{\omega Y}$. For additional information we also give in Table VI the values of R_{\max} which corresponds to the radius of neutron star with maximum mass. It is clear from the table that for smaller ζ the value of $R_{1.4}$ varies with Δr and is independent of $X_{\omega Y}$. This is due to the fact that for smaller ζ , central density for neutron star with mass $1.4M_{\odot}$ is lower or almost equal to the threshold density for hyperons (see also Fig. 7). But, as ζ increases, the central density becomes larger than the threshold densities for various hyperons, thus, $R_{1.4}$ depends on Δr as well as $X_{\omega Y}$. In Fig. 10 we plot the variations of R_{\max} and Z_{\max} versus the maximum neutron star mass. We see that the correlations in the values of M_{\max} and R_{\max} are stronger than the ones observed in the case of M_{\max} and $R_{1.4}$. The spread in the values of R_{\max} is only 0.2 ± 0.1 km for a fixed value of M_{\max} . The values of R_{\max} do not depend strongly on the choice of Δr as can be seen from Table VI. The horizontal line in the lower panel corresponds to the measured value of the redshift, $Z = 0.35$, for the neutron star EXO 0748-676 [53]. For $Z = 0.35$, we find that the M_{\max} is $\sim 1.8M_{\odot}$ and the corresponding radius is ~ 12 km. These values for neutron star masses and the corresponding radii are in reasonable agreement with the best suggested value of the mass $1.8M_{\odot}$ and radius 11.5 km corresponding to $Z=0.35$ [54].

To this end, we would like to mention that the calculations are repeated for an attractive $\Sigma - N$ potentials by assuming $U_{\Sigma}^{(N)} = -30$ MeV in Eq. (24). We find that with this choice of $U_{\Sigma}^{(N)}$ our results for the variations in the M_{\max} and $R_{1.4}$ do not get affected. However, the threshold density for Σ^{-} hyperon becomes lowest and Ξ^{-} hyperon does not appear even for the maximum neutron star mass. It must be pointed out that the tensor coupling of ω -meson to the hyperons, not considered in the present work, could increase the value of M_{\max} by about $0.1M_{\odot}$ [55]. We also remark that the effects due to the exchange and the correlations are not considered explicitly. But, they are taken into account at least partly

through the non-linear self and mixed interactions of the mesons [29, 30]. The Eqs. (11) - (16) can be interpreted as the Khon-Sham equations in relativistic case and in this sense they include effects beyond the Hartree approach through the non-linear couplings. However, a more accurate treatment of the exchange and correlation effects should be pursued [56, 57].

VI. ROTATING NEUTRON STARS

The properties of neutron stars can get significantly affected in the presence of rotation. The effects of rotation on the neutron star properties are pronounced when the frequency of rotation is close to its Keplerian limit. Earlier studies indicate that the Keplerian frequency is ~ 1000 Hz for the neutron stars with mass around $1M_{\odot}$ [58]. Only very recently [10], a neutron star rotating at 1122 Hz is discovered in the X-ray transient XTE J1739-285. In this section we shall discuss our results for the rotating neutron stars obtained using the extended FTRMF model. These results are obtained by solving the Einstein equations for stationary axi-symmetric spacetime. The numerical computations are performed using the code written by Stergioulas [59].

In Fig. 11 we plot the neutron star mass versus the circumferential equatorial radius R_{eq} for the Keplerian sequences obtained using EOSs for the LY, UY, L0 and U0 parameterizations of our model. The maximum mass of the neutron stars vary between $1.7 - 2.5M_{\odot}$ and $2.0 - 3.0M_{\odot}$ for the cases with and without the hyperons respectively. The values of $R_{\text{eq}}^{1.4}$ lie in the range of $18.4 - 20.0$ km irrespective of whether or not hyperonic degrees of freedom are included. Because, the central density for the canonical mass in the presence of rotation becomes lower than the threshold densities for the hyperons. The Keplerian frequencies at maximum neutron star mass for various cases shown in Fig. 11 lie in the range of $1320 - 1560$ Hz . This means that all the EOSs obtained in the present work can yield neutron stars rotating at 1122 Hz. In Fig. 12 we plot the mass and the corresponding values for R_{eq} for the neutron star rotating at 1122 Hz. The lower and upper bounds on the radii R_{eq} are determined by the setting-in of the axi-symmetric perturbation and mass-shedding instabilities, respectively [60]. The maximum values of R_{eq} are well fitted by [60]

$$R_{\text{eq}}^{\text{max}} = 13.87 \left(\frac{M}{M_{\odot}} \right)^{1/3} \text{ km} \quad (35)$$

which can be obtained using $\nu_k = 1122$ Hz and $\eta = 1$ in Eq. (32). In Table VII, we give

the minimum and maximum values for the R_{eq} and the corresponding neutron star mass for the various cases plotted in Fig. 12. We get $R_{\text{eq}}^{\text{min}} = 12.1 - 13.8$ km and $R_{\text{eq}}^{\text{max}} = 16.5 - 18.7$ km. The values of $M(R_{\text{eq}}^{\text{min}})$ and $M(R_{\text{eq}}^{\text{max}})$ are in the range of $1.6 - 2.7M_{\odot}$ and $1.7 - 2.6M_{\odot}$, respectively. The absolute difference between the $M(R_{\text{eq}}^{\text{min}})$ and $M(R_{\text{eq}}^{\text{max}})$ which gives the variations in the neutron star mass for a given EOS is at most $0.2M_{\odot}$. We also find that the baryonic mass for the neutron stars rotating with 1122 Hz for all the cases considered here are larger than the maximum baryonic mass for the corresponding non-rotating sequences. This suggests that the recently discovered fastest rotating neutron star rotating with 1122 Hz is supra massive. We also list in Table VII the values for the $r_{\text{pole}}/r_{\text{eq}}$ known as the flattening parameter and $T/|W|$ where T the kinetic energy and W the gravitational energy.

VII. CONCLUSIONS

We have used the extended FTRMF model to obtain a new set of EOSs with the different high density behaviour. These EOSs are then employed to study the variations in the properties of non-rotating and rotating neutron stars. The high density behaviour of the EOS which is not yet well constrained is varied by choosing the different values of the ω -meson self-coupling and the couplings of ω -meson to the various hyperons in our model. The different values for these couplings are so chosen that they span the entire range as often considered in the earlier works. The remaining parameters of the models are calibrated to yield reasonable fit to the bulk nuclear observables, nuclear matter incompressibility coefficient and hyperon-nucleon potential depths. The properties of finite nuclei and nuclear matter associated with each of the parameterizations used for obtaining EOSs can be summarized as follows. The rms errors for the total binding energies and charge radii calculated for the nuclei considered in the fits are $1.5 - 1.8$ MeV and $0.025 - 0.040$ fm. The binding energy per nucleon is 16.11 ± 0.04 MeV, saturation density is 0.148 ± 0.003 fm $^{-3}$ and nuclear matter incompressibility coefficient is 230.24 ± 9.80 MeV.

The values of M_{max} for the non-rotating neutron stars composed of nucleons and hyperons in β equilibrium can vary between $1.4 - 2.1M_{\odot}$. The radius $R_{1.4}$ for neutron star can vary in the range of $11.3 - 14.1$ km. The values of $R_{1.4}$ narrow down to only $12.8 - 14.1$ km if one considers the EOSs for which M_{max} is larger than $1.6M_{\odot}$ as it is the highest mass measured

for PSR J0751+1807 with 95% confidence limit. This result is in reasonable agreement with $R_{1.4} = 14.8_{-1.6}^{+1.8}$ km as deduced very recently by adequately fitting the high quality X-ray spectrum from the neutron star X7 in the globular cluster 47 Tucanae [52]. We also note strong correlations between the values of M_{max} and $R_{1.4}$. The values of the redshift for the neutron stars with canonical and maximum masses are also calculated. The redshift for the neutron star with canonical mass obtained for different EOSs varies in between 0.19 – 0.25. The maximum value for the redshift is 0.41 which corresponds to the maximum neutron star mass of $2.1M_{\odot}$. For the measured value of redshift equal to 0.35, we find that the neutron star mass is $\sim 1.8M_{\odot}$ and the corresponding radius is ~ 12 km. These values for neutron star masses and the corresponding radii are in reasonable agreement with the best suggested value of the mass $1.8M_{\odot}$ and radius 11.5 km for $Z=0.35$ [54]. For the sake of comparison we have presented our results obtained without the inclusions of the hyperons. In this case the M_{max} and $R_{1.4}$ lie in the range of $1.7 - 2.4M_{\odot}$ and $12.5 - 14.1$ km, respectively.

We use our EOSs to compute the properties of the rotating neutron stars. In particular, we studied the mass and the circumferential equatorial radius for the neutron star rotating at 1122 Hz as recently observed [10]. Our results for different EOSs indicate that the mass for such a star can lie within $1.6 - 2.7M_{\odot}$. The minimum values for the circumferential equatorial radius determined by the onset of the instability with respect to the axi-symmetric perturbation are found to vary in the range of 12.1 – 13.8 km. The maximum values for the circumferential equatorial radius obtained by the mass-shedding limit vary within 16.5–18.7 km. Looking into the results for the baryonic mass we find that the neutron star rotating at 1122 Hz are supra massive for our EOSs.

Acknowledgments

We would like to thank D. Bandyopadhyay for useful discussions. This work was supported in part by the University Grant Commission under grant # F.17-40/98 (SA-I). Shashi K. Dhiman and Raj Kumar greatly acknowledge the financial support from Saha Institute of Nuclear Physics, Kolkata, India.

-
- [1] S. E. Thorsett and D. Chakrabarty, *Astrophys. J* **512**, 288 (1999).
- [2] M. Burgay, N. D’Amico, A. Possenti, R. N. Manchester, A. G. Lyne, B. C. Joshi, M. A. McLaughlin, F. C. M. Kramer, J. M. Sarkissian, V. Kalogera, C. Kim, et al., *Nature* **426**, 531 (2003).
- [3] A. Lyne *et al*, *Science* **303**, 1153 (2004).
- [4] D. J. Nice, E. Splaver, I. Stairs, O. Lohmer, A. J. A. Jessner, M. Kramer, and J. Cordes, *Astrophys. J.* **634**, 1242 (2005).
- [5] R. Rutledge, L. Bildsten, E. Brown, G. Pavlov, and V. Zavlin, *Astrophys. J.* **578**, 405 (2002).
- [6] R. Rutledge, L. Bildsten, E. Brown, G. Pavlov, and V. Zavlin, *Astrophys. J.* **577**, 346 (2002).
- [7] B. Gendre, D. Barret, and N. A. Webb, *Astrono. Astrophys.* **400**, 521 (2003).
- [8] W. Becker and et al., *Astrophys. J.* **594**, 364 (2003).
- [9] J. Cottam, F. Paerels, and M. Mendez, *Nature* **420**, 51 (2002).
- [10] P. Kaaret, Z. Prieskorn, J. in ’t Zand, S. Brandt, N. Lund, S. Mereghetti, D. Gotz, E. Kuulkers, and J. Tomsick, *Astrophys. J.* **657**, L97 (2006).
- [11] G. Lavagetto, I. Bombaci, A. D’Ai’, I. Vidana, and N. Robba, astro-ph/0612061 (2006).
- [12] V. R. Pandharipande and R. A. Smith, *Nucl. Phys.* **A237**, 507 (1975).
- [13] E. Chabanat, P. Bonche, P. Haensel, J. Meyer, and R. Schaeffer, *Nucl. Phys.* **A627**, 710 (1997).
- [14] J. R. Stone, J. C. Miller, R. Koncewicz, P. D. Stevenson, and M. R. Strayer, *Phys. Rev. C* **68**, 034324 (2003).
- [15] L. Monras, *Eur. Phys. J.* **A24**, 293 (2005).
- [16] B. K. Agrawal, S. K. Dhiman, and R. Kumar, *Phys. Rev. C* **73**, 034319 (2006).
- [17] M. Prakash, J. R. Cooke, and J. M. Lattimer, *Phys. Rev. D* **52**, 661 (1995).
- [18] N. K. Glendenning and J. Schaffner-Bielich, *Phys. Rev. C* **60**, 025803 (1999).
- [19] A. W. Steiner, M. Prakash, J. M. Lattimer, and P. Ellis, *Phys. Rep.* **411**, 325 (2005).
- [20] H. Mütter, M. Prakash, and T. L. Ainsworth, *Phys. Lett.* **B199**, 469 (1987).
- [21] L. Engvik, M. Hjorth-Jensen, E. Osnes, G. Bao, and E. Østgaard, *Phys. Rev. Lett.* **73**, 2650 (1994).
- [22] L. Engvik, E. Osnes, M. Hjorth-Jensen, G. Bao, and E. Østgaard, *Astrophys. J.* **469**, 794

- (1996).
- [23] H. J. Schulze, A. Polls, A. Ramos, and I. Vidana, *Phys. Rev. C* **73**, 058801 (2006).
 - [24] H. Müller and B. D. Serot, *Nucl. Phys.* **A606**, 508 (1996).
 - [25] A. R. Taurines, C. A. Z. Vasconcellos, M. Malherio, and M. Chiapparini, *Phys. Rev. C* **63**, 065801 (2001).
 - [26] T. K. Jha, P. K. Raina, P. K. Panda, and S. K. Patra, *Phys. Rev. C* **74**, 055803 (2006).
 - [27] P. G. Reinhard, *Nucl. Phys.* **A649**, 305c (1999).
 - [28] D. H. Youngblood, Y.-W. Lui, and H. L. Clark, *Phys. Rev. C* **65**, 034302 (2002).
 - [29] R. Furnstahl, B. D. Serot, and H.-B. Tang, *Nucl. Phys.* **A598**, 539 (1996).
 - [30] R. Furnstahl, B. D. Serot, and H.-B. Tang, *Nucl. Phys.* **A615**, 441 (1997).
 - [31] B. D. Serot and J. D. Walecka, *Int. J. Mod. Phys. E* **6**, 515 (1997).
 - [32] C. J. Horowitz and J. Piekarewicz, *Phys. Rev. Lett.* **86**, 5647 (2001).
 - [33] R. Furnstahl, *Nucl. Phys.* **A706**, 85 (2002).
 - [34] T. Sil, M. Centelles, X. Vinas, and J. Piekarewicz, *Phys. Rev.* **C71**, 045502 (2005).
 - [35] J. M. Lattimer, C. J. Pethick, M. Prakash, and P. Haensel, *Phys. Rev. Lett.* **66**, 2701 (1991).
 - [36] Y. Sugahara and H. Toki, *Nucl. Phys.* **A579**, 557 (1994).
 - [37] L.-W. Chen, C. M. Ko, and B.-A. Li, *Phys. Rev. C* **72**, 064309 (2005).
 - [38] B. K. Agrawal, S. Shlomo, and V. K. Au, *Phys. Rev. C* **72**, 014310 (2005).
 - [39] R. Kumar, B. K. Agrawal, and S. K. Dhiman, *Phys. Rev. C* **74**, 034323 (2006).
 - [40] I. Bednarek and R. Manka, *J. Phys. G* **31**, 1009 (2005).
 - [41] J. Schaffner and A. Gal, *Phys. Rev. C* **62**, 034311 (2000).
 - [42] N. K. Glendenning and S. A. Moszkowski, *Phys. Rev. Lett.* **67**, 2414 (1991).
 - [43] G. A. Lalazissis, J. König, and P. Ring, *Phys. Rev. C* **55**, 540 (1997).
 - [44] S. Weinberg, *Gravitation and Cosmology* (Wiley, New York, 1972).
 - [45] G. Baym, C. Pethick, and P. Sutherland, *Astrophys. J.* **170**, 299 (1971).
 - [46] J. M. Lattimer, M. Prakash, D. Masak, and A. Yahil, *Astrophys. J.* **355**, 241 (1990).
 - [47] J. M. Lattimer and M. Prakash, *Astrophys. J.* **550**, 426 (2001).
 - [48] J. M. Lattimer and M. Prakash, *Science* **304**, 536 (2004).
 - [49] J. Schaffner and I. N. Mishustin, *Phys. Rev. C* **53**, 1416 (1996).
 - [50] H. Shen, *Phys. Rev. C* **65**, 035802 (2002).
 - [51] M. Bejger, T. Bulik, and P. Haensel, *Mon. Not. R. Astron. Soc.* **364**, 635 (2005).

- [52] C. O. Heinke, G. B. Rybicki, R. Narayan, and J. E. Grindlay, *Astrophys. J.* **644**, 1090 (2006).
- [53] F. Ozel, *Nature* **441**, 1115 (2006).
- [54] A. R. Villarreal and T. E. Strohmayer, *Astrophys. J.* **614**, L121 (2004).
- [55] Y.Sugahara and H.Toki, *Prog. Theor. Phys* **92**, 803 (1994).
- [56] V. Greco, F. Matera, M. Colonna, M. Di Toro, and G. Fabbri, *Phys. Rev.C* **63**, 035202 (2001).
- [57] P. K. Panda, J. da Providncia, and C. Providncia, *Phys. Rev. C* **73**, 035805 (2006).
- [58] S. L. Shapiro and S. A. Teukolsky, *Black Holes, White Dwarfs, and Neutron Stars* (Wiley, New York, 1983).
- [59] N. Stergioulas and J. L. Friedman, *Astrophys. J.* **444**, 306 (1995).
- [60] M. Bejger, P. Haensel, and J. Zdunik, *Astro.Astrophys.* **464**, L49 (2007).
- [61] P. Danielewicz, R. Lacey, and G. Lynch, *Science* **298**, 1592 (2002).

FIG. 1: (Color online) Variations of $X_{\sigma Y}$ with $X_{\omega Y}$ for Λ , Σ and Ξ hyperons. The values of $X_{\sigma Y}$ for a given value of $X_{\omega Y}$ are calculated using Eqs. (24 and 26).

FIG. 2: (Color online) Variations of the symmetry energy coefficient J (upper panel) and its linear density dependence L (lower panel) as a function of Δr for different parameterizations with $\zeta = 0.0, 0.03$ and 0.06 .

FIG. 3: (Color online) Variations of the rms errors in the total binding energies (upper panel) and charge rms radii (lower panel) as a function of Δr for different parameterizations with $\zeta = 0.0, 0.03$ and 0.06 .

FIG. 4: (Color online) The EOSs for pure neutron matter (upper panel) and symmetric nuclear matter (lower panel). The solid and dashed curves correspond to $\Delta r = 0.16$ and 0.28 fm, respectively. The shaded regions represent the experimental data taken from Ref. [61].

FIG. 5: (Color online) The chemical potentials for neutron (upper panel) and electron (lower panel) as a function of density.

FIG. 6: (Color online) Variation of neutron star mass as a function of its radius R for selected EOSs. These EOSs are obtained using the parameter sets LY (UY) correspond to combinations of $\Delta r = 0.16(0.28)$, $\zeta = 0.06(0.0)$ and $X_{\omega Y} = 0.5(0.8)$. The parameter sets L0 and U0 are analogous to LY and UY respectively, but, with no hyperons. The various constraints as indicated by causality, rotation, and $\Delta I/I = 0.014$ are discussed in the text.

FIG. 7: (Color online) The threshold density for various hyperons and central densities for neutron star with the canonical mass and maximum mass obtained for the EOSs corresponding to the parameter sets LY and UY.

FIG. 8: (Color online) Particle fractions as a function of radial coordinate of the neutron star obtained at maximum mass for LY (upper panel) and UY (lower panel) parameterizations. The curves labeled as "n/3" should be multiplied by three to get the actual neutron fractions.

FIG. 9: (Color online) Variations of radius ($R_{1.4}$) and redshift ($Z_{1.4}$) for neutron star with the canonical mass as a function of maximum neutron star mass obtained for the EOSs corresponding to the all different parameterizations of the extended FTRMF model as considered. The vertical line at $M_{\max} = 1.6M_{\odot}$ in the upper panel corresponds to the mass of the PSR J0751+1807 measured with 95% confidence limit.

FIG. 10: (Color online) Variations of radius (R_{\max}) and redshift (Z_{\max}) for neutron star with the maximum mass as a function of maximum neutron star mass obtained for the EOSs corresponding to the all different parameterizations of the extended FTRMF model as considered. The horizontal line in the lower panel corresponds to the measured value of the redshift, $Z = 0.35$, for the neutron star EXO 0748-676 [53].

FIG. 11: (Color online) The relationship between mass M and the circumferential equatorial radius R_{eq} for Keplerian sequences for different EOSs obtained within the extended FTRMF model.

FIG. 12: (Color online) The mass M verses the circumferential equatorial radius R_{eq} for the neutron stars rotating at 1122 Hz for selected EOSs obtained within the extended FTRMF model. The minimum values for the radius indicated by open circles are determined by the setting-in of the instability with respect to axi-symmetric perturbations. The maximum values for the radius indicated by open squares are determined by the mass-shedding instability. The values of maximum radius are well fitted by solid curve obtained using Eq.(35).

TABLE I: New coupling strength parameters for the Lagrangian of the extended FTRMF model as given in Eq.(1). The seven different parameter sets correspond to the different values of the neutron skin-thickness Δr for the ^{208}Pb nucleus used in the fit. The value of ω -meson self-coupling ζ is equal to 0.0 for all these parameterizations. The values of Δr are in fm, the parameters $\bar{\kappa}$, $\bar{\alpha}_1$, and $\bar{\alpha}_2$ are in fm^{-1} and m_σ are in MeV. The masses for other mesons are taken to be $m_\omega = 782.5$ MeV, $m_\rho = 763$ MeV, $m_\sigma^* = 975$ MeV and $m_\phi = 1020$ MeV. For the masses of nucleons and hyperons we use $M_N = 939$ MeV, $M_\Lambda = 1116$ MeV, $M_\Sigma = 1193$ MeV and $M_\Xi = 1313$ MeV. The values of $\bar{\kappa}$, $\bar{\lambda}$, $\bar{\alpha}_1$, $\bar{\alpha}'_1$, $\bar{\alpha}_2$, $\bar{\alpha}'_2$, and $\bar{\alpha}'_3$ are multiplied with 10^2 .

Δr	0.16	0.18	0.20	0.22	0.24	0.26	0.28
$g_{\sigma N}$	10.51369	10.65616	10.44426	10.50339	10.34061	10.48597	10.32009
$g_{\omega N}$	13.48789	13.95799	13.52239	13.80084	13.46209	13.81202	13.45113
$g_{\rho N}$	14.98497	14.32687	13.11709	12.12975	11.18278	10.39449	10.09608
$\bar{\kappa}$	2.62556	3.02154	2.43049	3.39711	3.24752	3.05611	2.82791
$\bar{\lambda}$	-0.73495	-0.45437	-0.04279	-1.15784	-1.36867	-0.86772	-1.13890
$\bar{\alpha}_1$	0.22672	0.38665	0.18121	0.44021	0.35304	0.34843	0.23357
$\bar{\alpha}'_1$	0.07325	0.07791	0.15979	0.00987	0.00725	0.052231	0.04733
$\bar{\alpha}_2$	3.05925	2.91796	2.96668	2.56759	2.27472	0.68086	0.60739
$\bar{\alpha}'_2$	1.55587	1.35016	1.25303	0.51396	0.15515	0.41389	0.33057
$\bar{\alpha}'_3$	1.50060	1.47585	0.09727	1.04562	0.52777	1.14566	0.30434
m_σ	502.23217	495.76339	497.83489	491.48257	492.76821	490.24238	491.86681

TABLE II: Same as Table I, but, with ω -meson self coupling $\zeta = 0.03$.

Δr	0.16	0.18	0.20	0.22	0.24	0.26	0.28
$g_{\sigma N}$	10.62886	10.76147	10.73005	10.71942	10.61808	10.67656	10.60110
$g_{\omega N}$	13.65991	14.11102	14.04275	14.12534	13.88708	14.11958	14.03101
$g_{\rho N}$	14.99076	14.67414	13.69014	12.19156	10.96456	10.14811	10.00441
$\bar{\kappa}$	1.38118	1.56065	1.62316	1.61820	1.77184	1.68916	1.78793
$\bar{\lambda}$	0.58536	0.97528	0.64498	1.06102	0.48269	0.86649	0.74676
$\bar{\alpha}_1$	0.00366	0.10311	0.08281	0.10650	0.12586	0.11999	0.16088
$\bar{\alpha}'_1$	0.02717	0.05071	0.02980	0.06526	0.00052	0.04411	0.01669
$\bar{\alpha}_2$	2.89393	3.06821	3.18222	2.77747	1.18745	0.68168	0.47146
$\bar{\alpha}'_2$	1.59659	1.16255	0.47540	0.22126	1.27574	0.54787	0.52816
$\bar{\alpha}'_3$	1.52088	1.35981	0.97721	0.45581	0.28975	0.35906	0.32358
m_σ	506.50582	500.51106	499.52635	497.20745	499.12460	495.18211	494.93882

TABLE III: Same as Table I, but, with ω -meson self coupling $\zeta = 0.06$.

Δr	0.16	0.18	0.20	0.22	0.24	0.26	0.28
$g_{\sigma N}$	11.05170	11.02412	10.95765	11.01908	10.91944	11.10806	11.03151
$g_{\omega N}$	14.65579	14.66595	14.59582	14.77458	14.64700	15.19792	15.01572
$g_{\rho N}$	14.98725	14.52186	13.41111	11.94837	10.71055	10.08835	10.00666
$\bar{\kappa}$	0.66576	0.69497	0.76852	0.78002	0.90221	1.13349	0.80797
$\bar{\lambda}$	2.46427	2.44874	2.41259	2.47238	2.33265	2.51229	2.41320
$\bar{\alpha}_1$	0.00601	0.00449	0.00409	0.01469	0.03499	0.14153	0.02073
$\bar{\alpha}'_1$	0.00203	0.00526	0.01079	0.01559	0.00230	0.00085	0.01109
$\bar{\alpha}_2$	2.86236	2.58355	2.66308	2.02292	1.24695	1.18538	0.55325
$\bar{\alpha}'_2$	1.55176	1.56881	1.30876	0.90169	0.77919	0.27422	0.16326
$\bar{\alpha}'_3$	1.55307	1.58487	0.84916	0.96305	0.74863	0.40699	0.72768
m_σ	503.43838	501.37038	499.38134	497.27203	495.82388	490.83495	490.68907

TABLE IV: The values of central baryon density ρ_c , mass M , radius R , radiation radius R_∞ , binding energy E_{bind} and redshift Z for non-rotating neutron stars with maximum mass calculated for the EOSs obtained using LY, UY, L0 and U0 parameterizations. The parameter sets LY (L0) and UY (U0) yield softest and stiffest EOS with (without) hyperons in comparison to all other parameterizations obtained in Sec. III.

	<i>LY</i>	<i>UY</i>	<i>L0</i>	<i>U0</i>
ρ_c (fm ⁻³)	1.05	0.84	1.12	0.79
$M(M_\odot)$	1.4	2.1	1.7	2.4
R (km)	11.3	12.0	10.9	12.2
R_∞ (km)	14.2	17.3	14.9	18.9
E_{bind} (10 ⁵³ ergs)	1.36	3.80	2.76	6.49
Z	0.25	0.41	0.37	0.57

TABLE V: Same as Table IV, but, for the non-rotating neutron stars with canonical mass.

	<i>LY</i>	<i>UY</i>	<i>L0</i>	<i>U0</i>
ρ_c (fm ⁻³)	1.05	0.32	0.50	0.32
R (km)	11.3	14.1	12.5	14.1
R_∞ (km)	14.2	16.8	15.3	16.8
E_{bind} (10 ⁵³ ergs)	1.36	1.10	1.37	1.10
Z	0.25	0.19	0.22	0.19

TABLE VI: Values of the M_{\max} , $R_{1.4}$ and the radius R_{\max} for the neutron star with maximum mass obtained for the EOSs corresponding to the selected combinations of Δr , ζ and $X_{\omega Y}$.

$X_{\omega Y}$	Δr	$\zeta = 0.0$			$\zeta = 0.06$		
		M_{\max}	$R_{1.4}$	R_{\max}	M_{\max}	$R_{1.4}$	R_{\max}
	(fm)	(M_{\odot})	(km)	(km)	(M_{\odot})	(km)	(km)
0.50	0.16	1.8	13.4	12.0	1.4	11.3	11.3
	0.28	1.8	14.1	12.2	1.4	11.6	11.6
0.80	0.16	2.1	13.4	12.0	1.5	12.3	11.0
	0.28	2.1	14.1	12.1	1.5	13.0	11.3

TABLE VII: The properties of neutron star rotating with 1122 Hz for different EOSs calculated within FTRMF model.

EOS	$M(R_{\text{eq}}^{\min})$	R_{eq}^{\min}	$r_{\text{pole}}/r_{\text{eq}}$	$T/ W $
	(M_{\odot})	(km)		
L0	1.908	12.12	0.804	0.054
U0	2.721	13.46	0.815	0.063
LY	1.624	13.85	0.692	0.076
UY	2.266	12.99	0.799	0.059
EOS	$M(R_{\text{eq}}^{\max})$	R_{eq}^{\max}	$r_{\text{pole}}/r_{\text{eq}}$	$T/ W $
	(M_{\odot})	(km)		
L0	1.909	17.14	0.566	0.109
U0	2.556	18.73	0.556	0.127
LY	1.694	16.49	0.575	0.097
UY	2.360	18.35	0.559	0.118

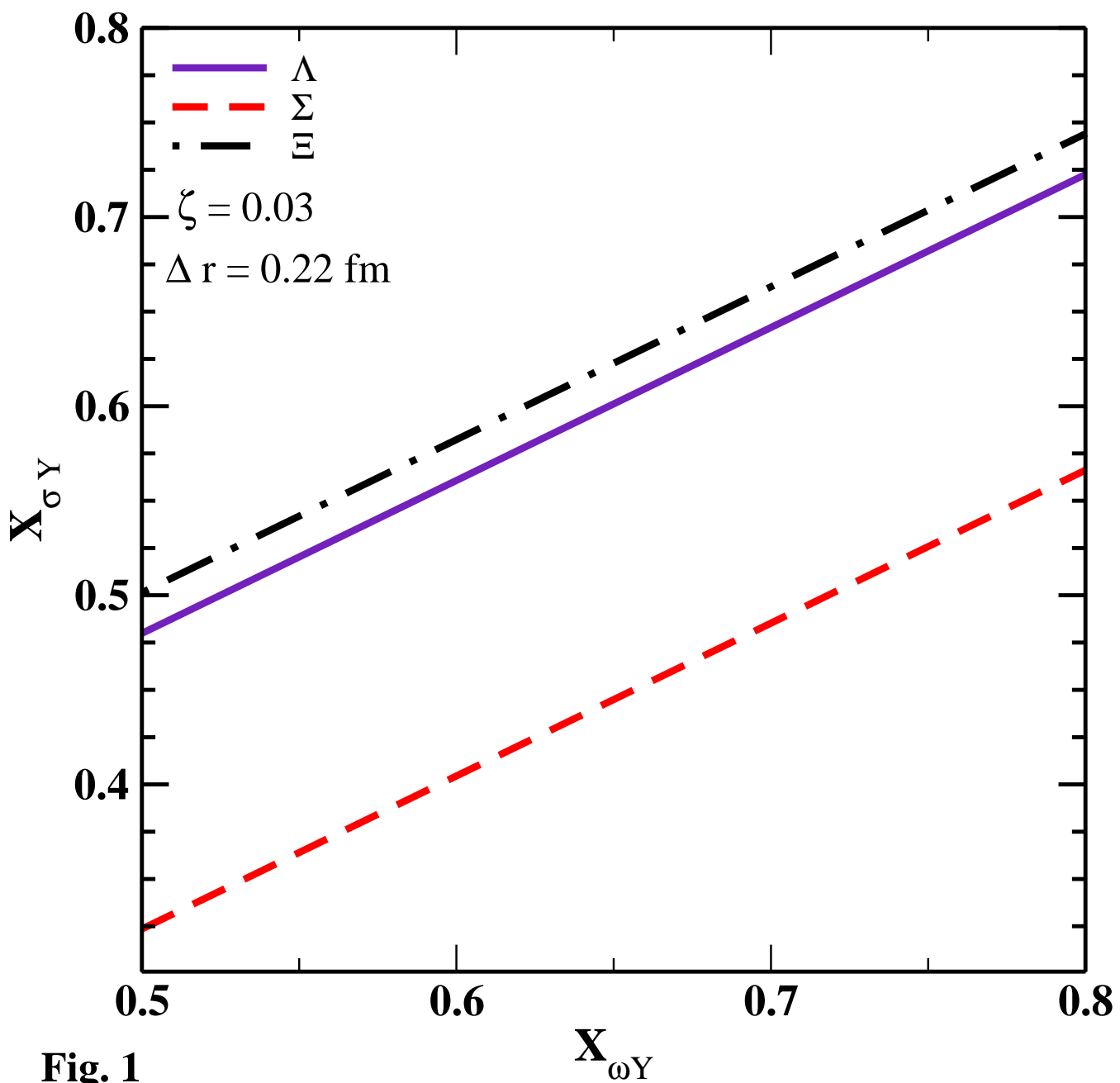


Fig. 1

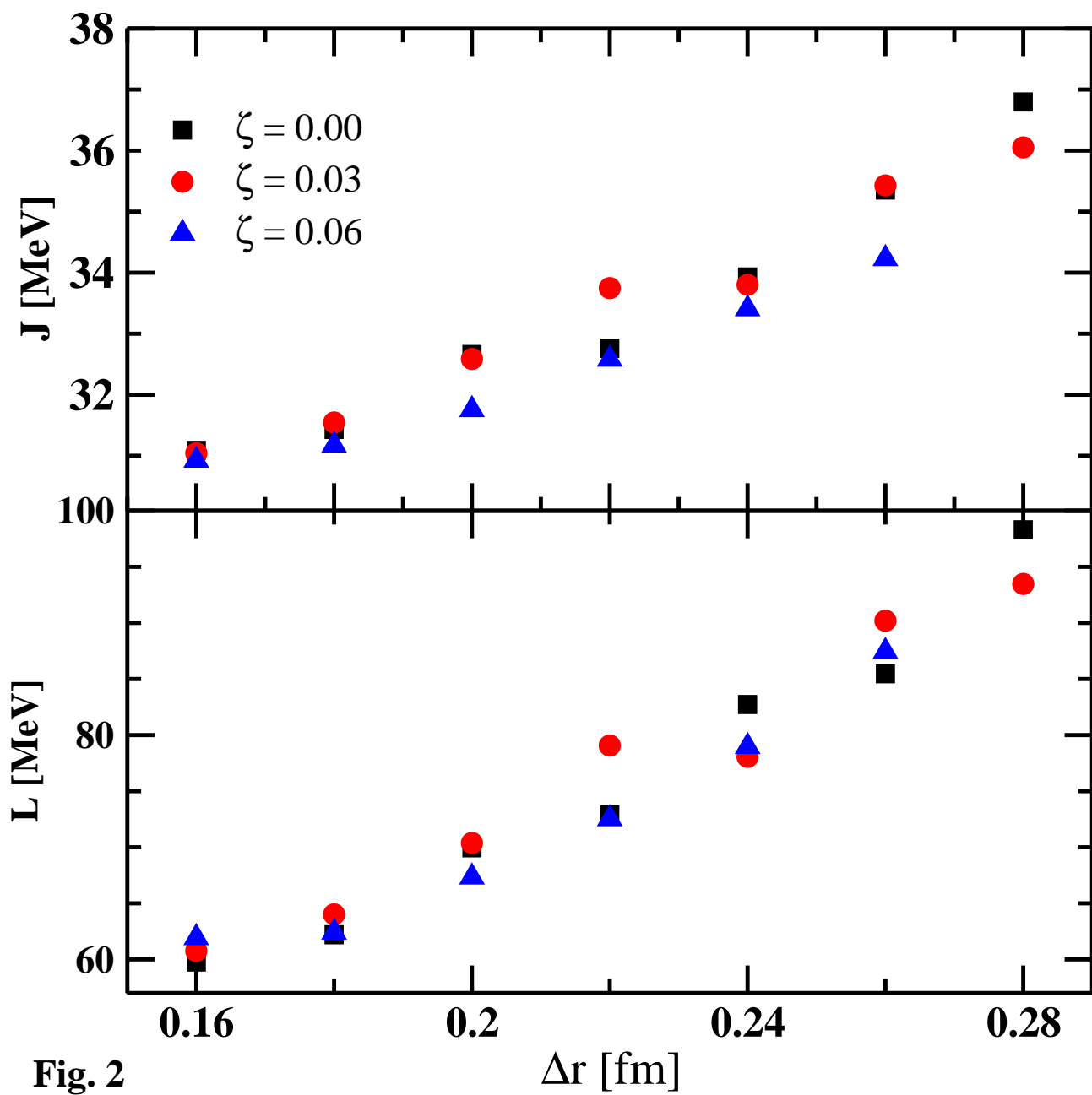


Fig. 2

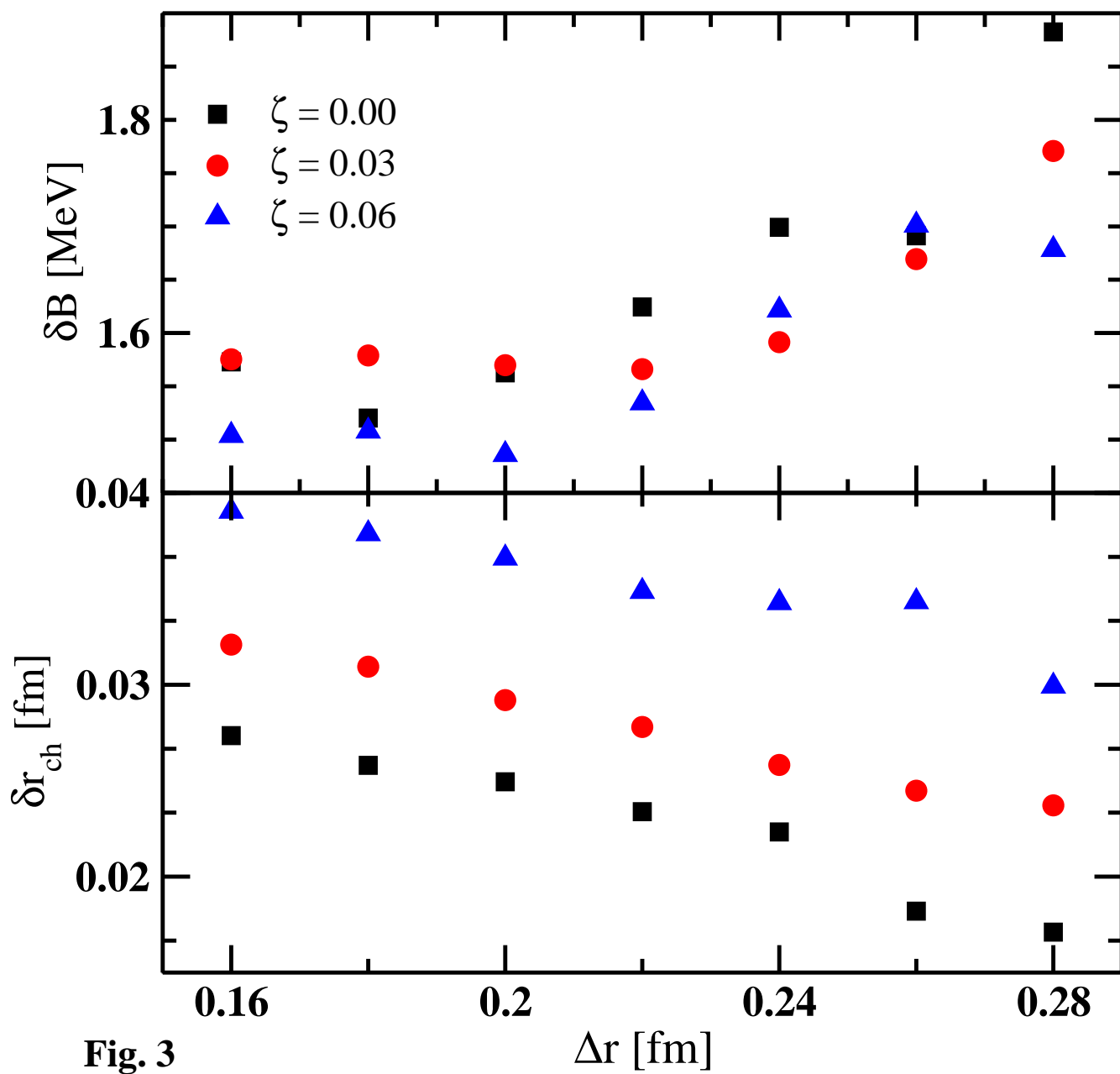


Fig. 3

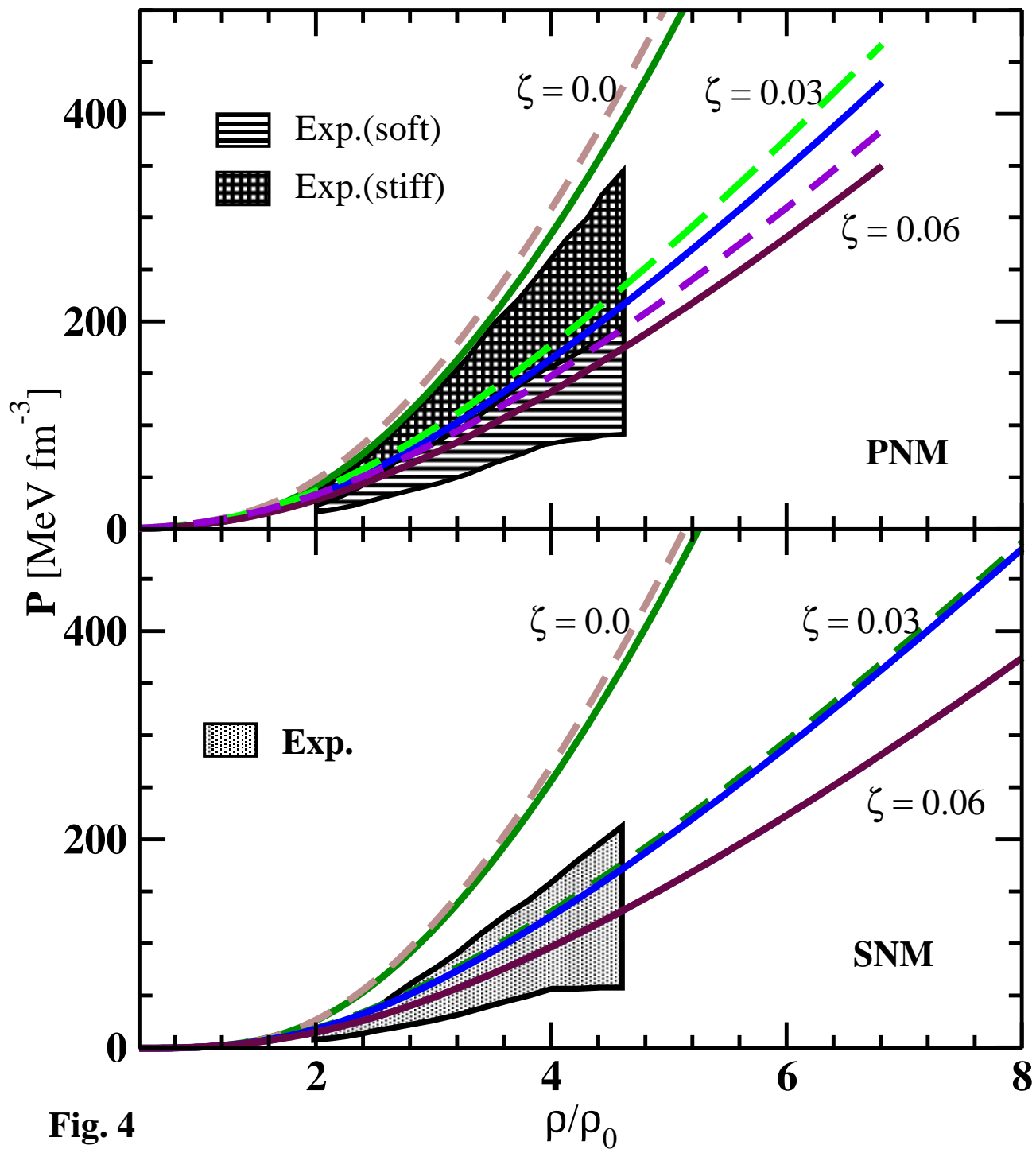
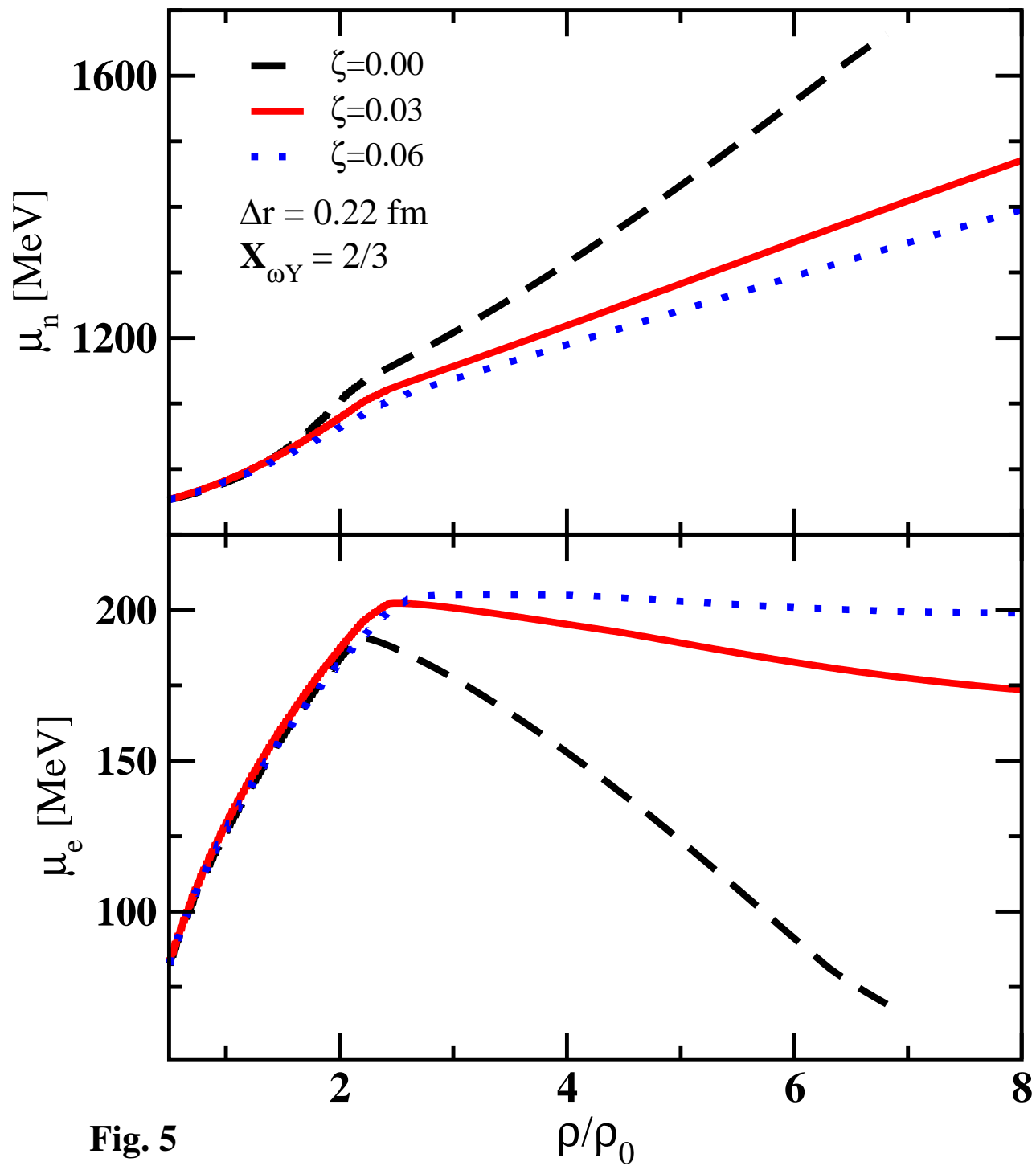


Fig. 4



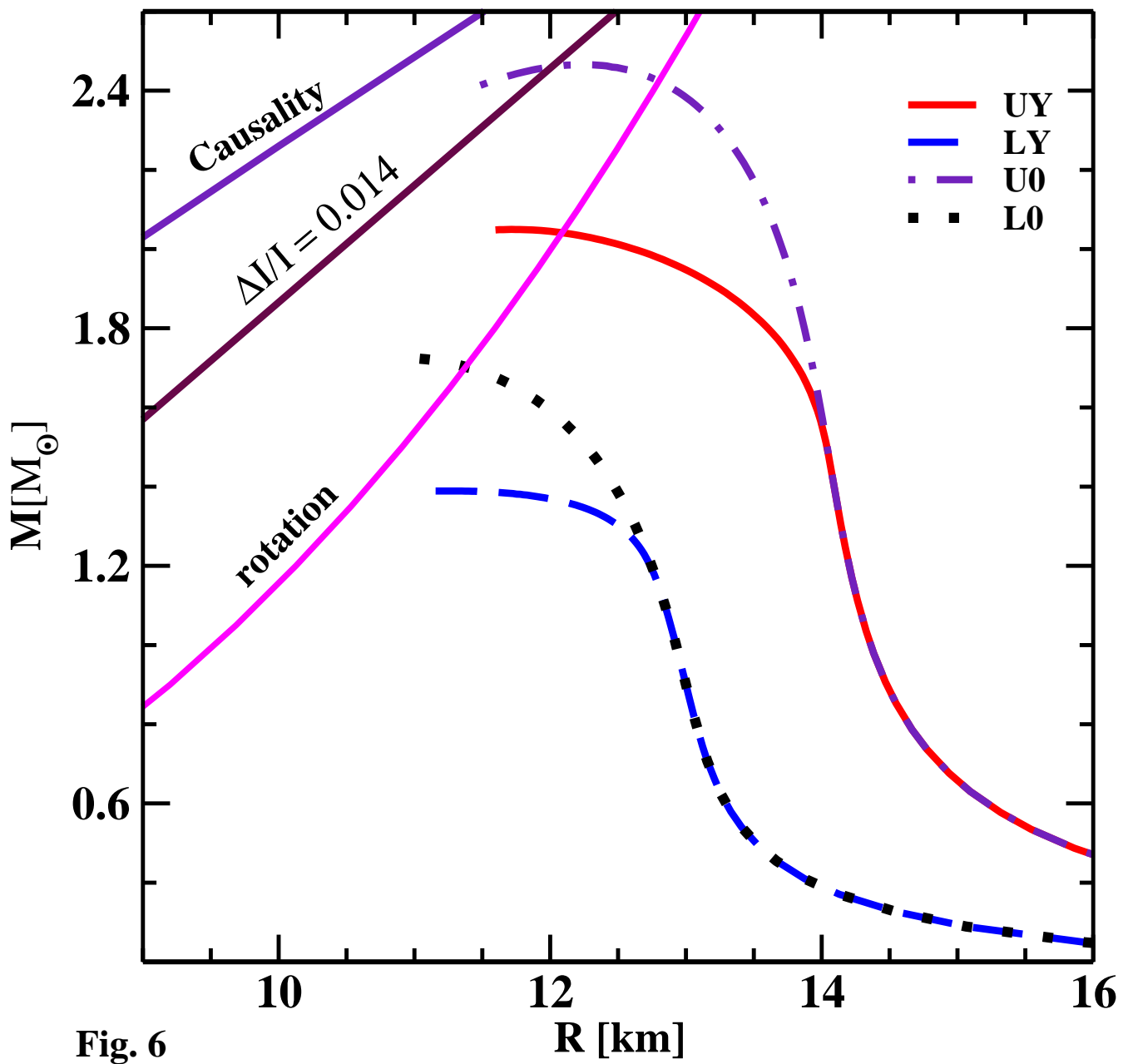


Fig. 6

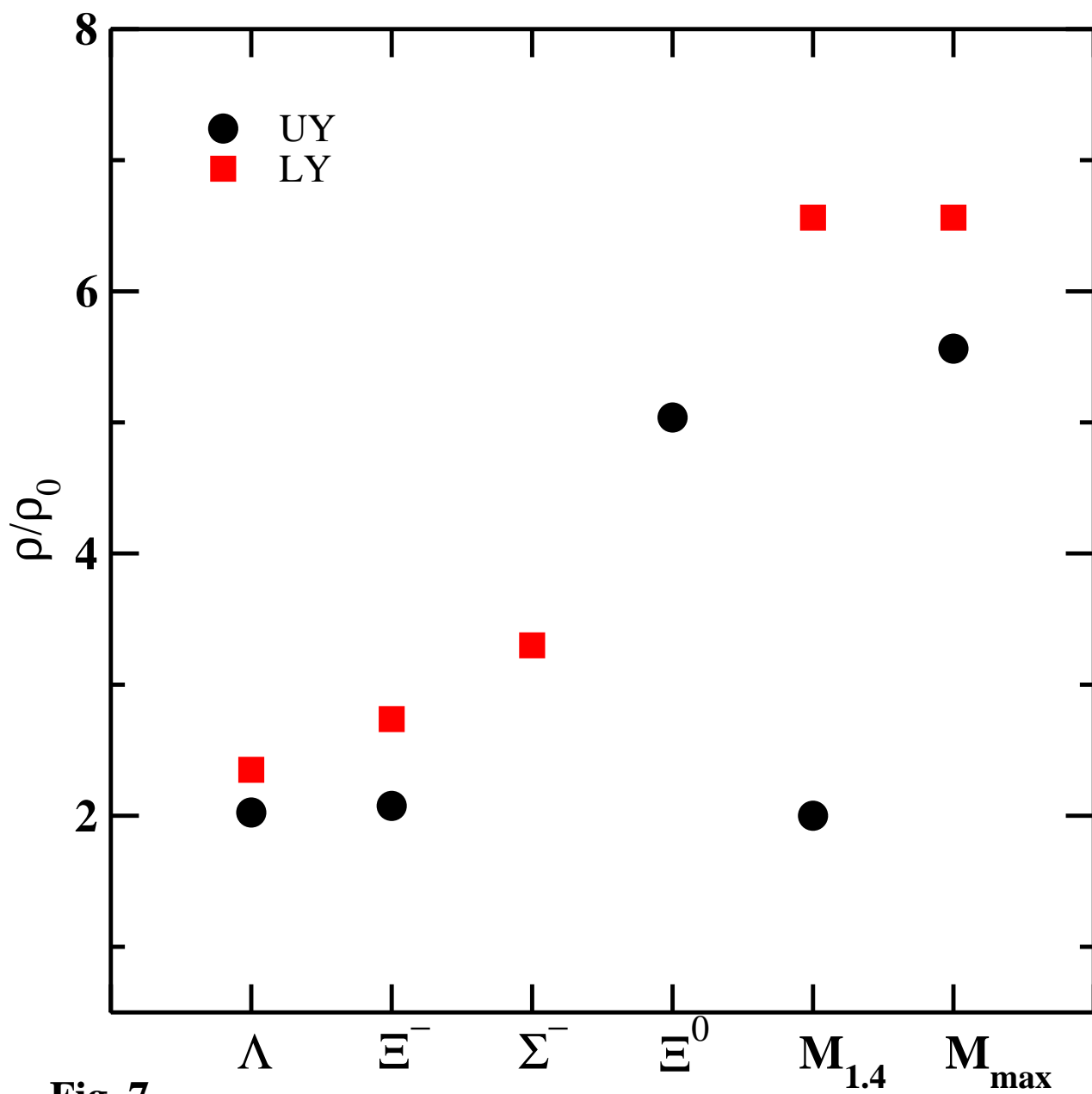


Fig. 7

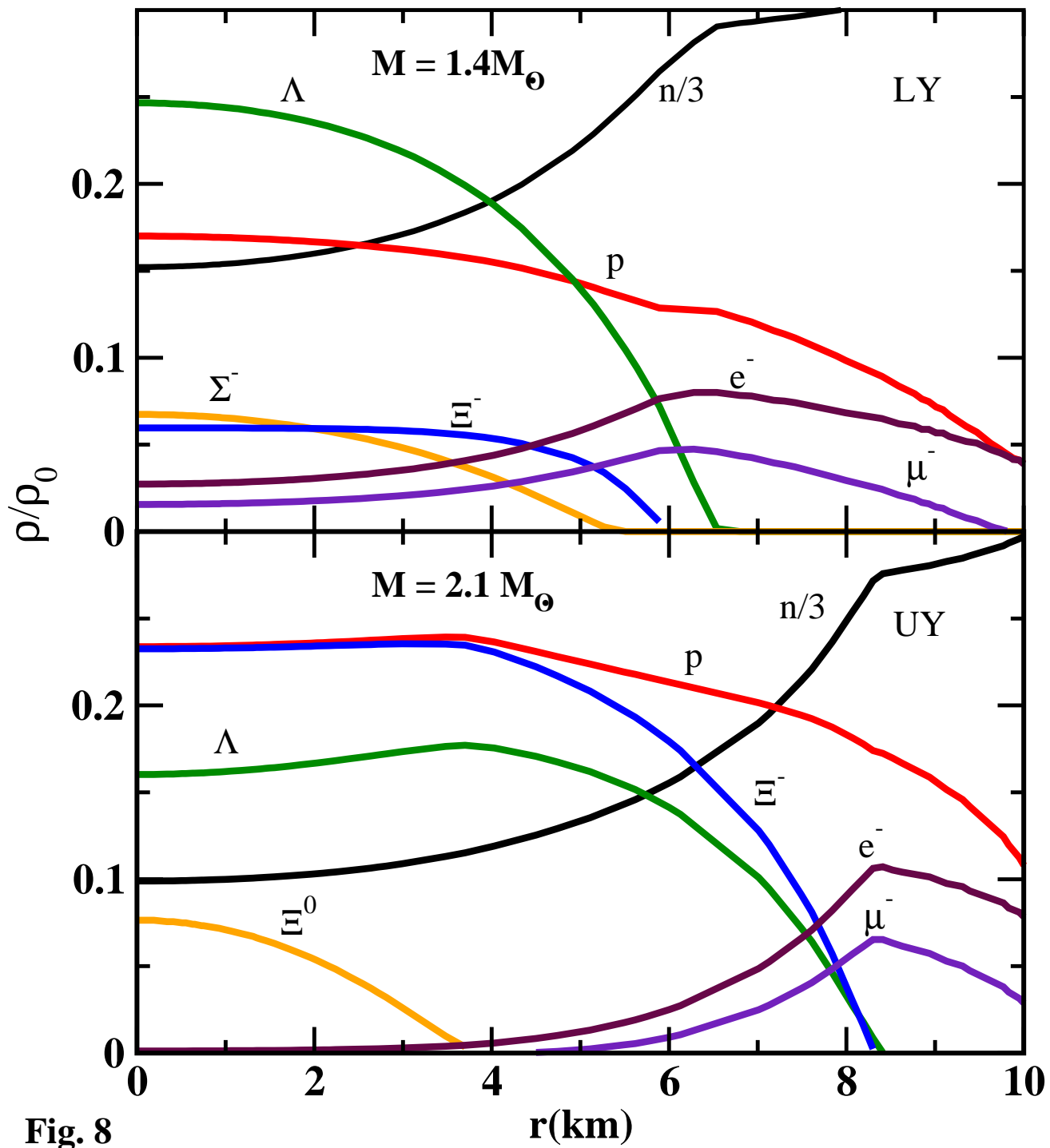


Fig. 8

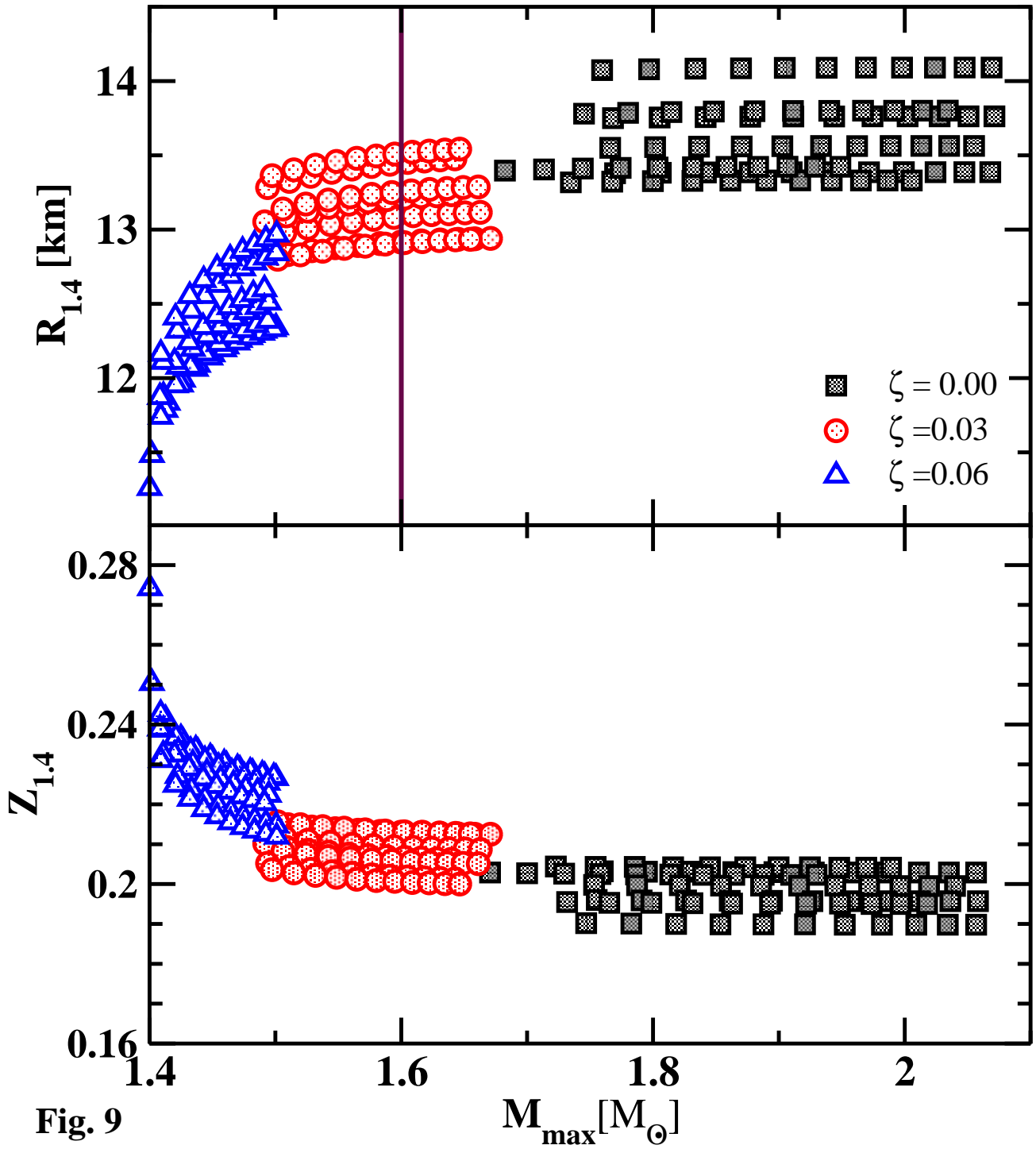


Fig. 9

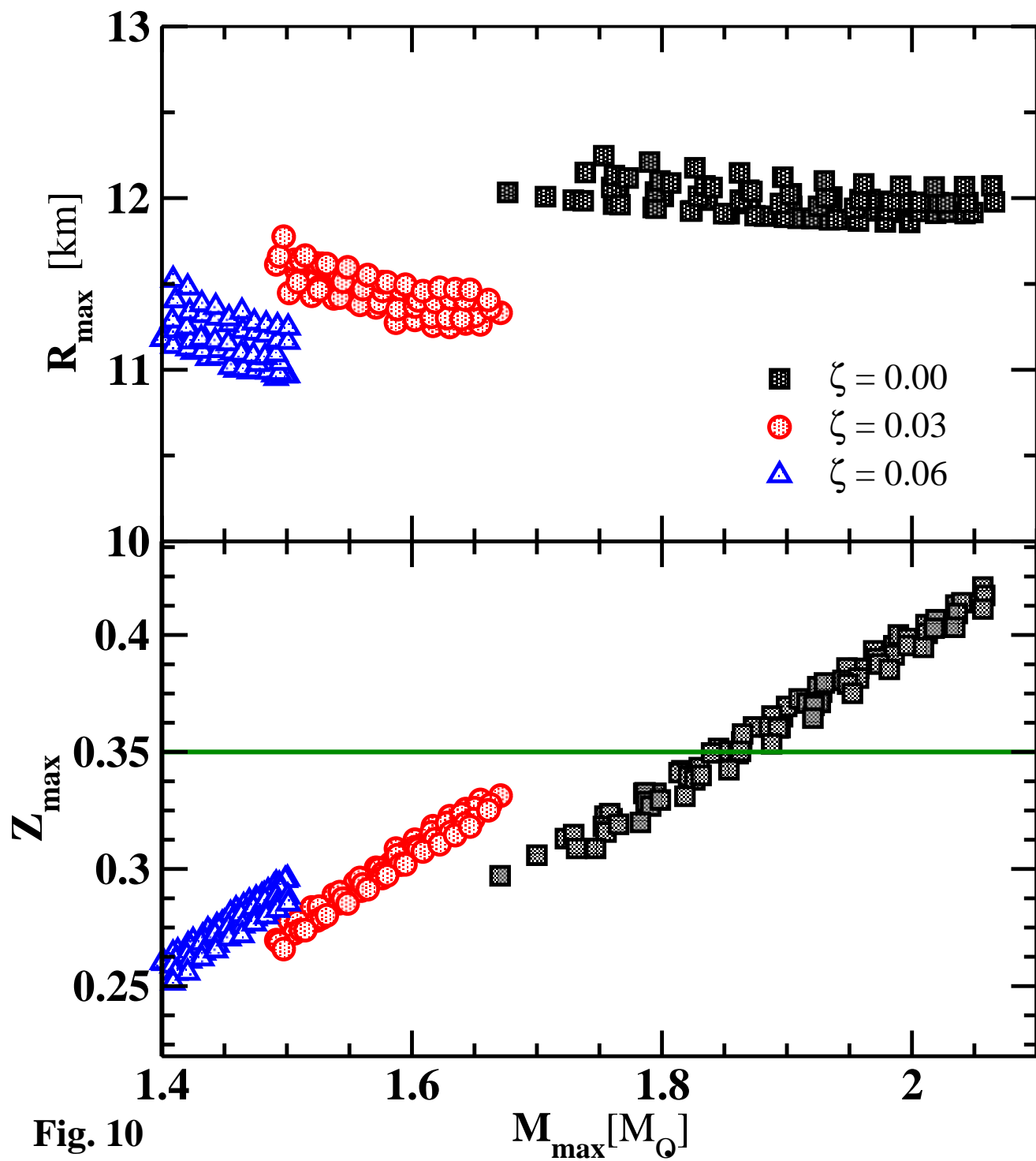


Fig. 10

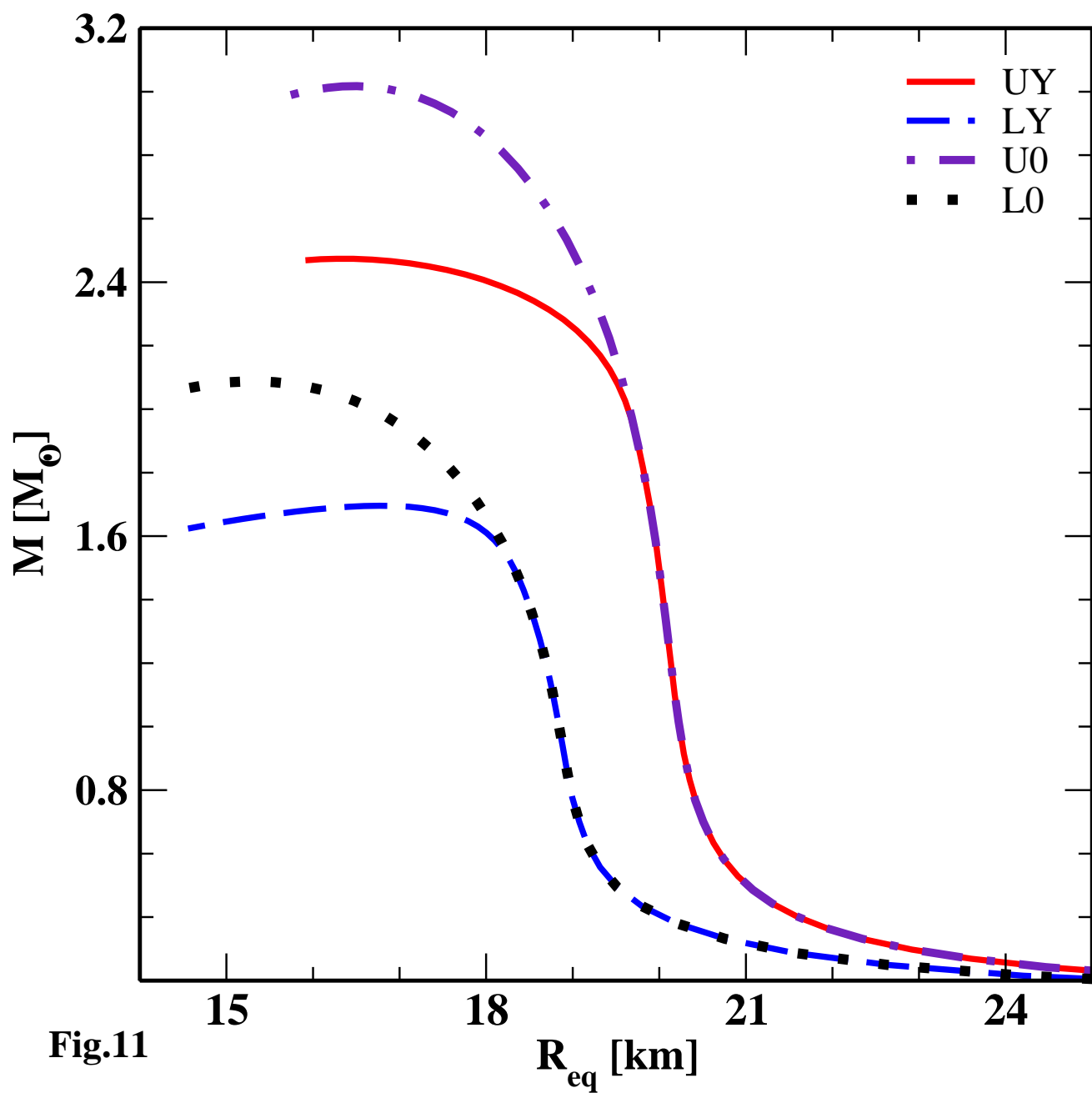


Fig.11

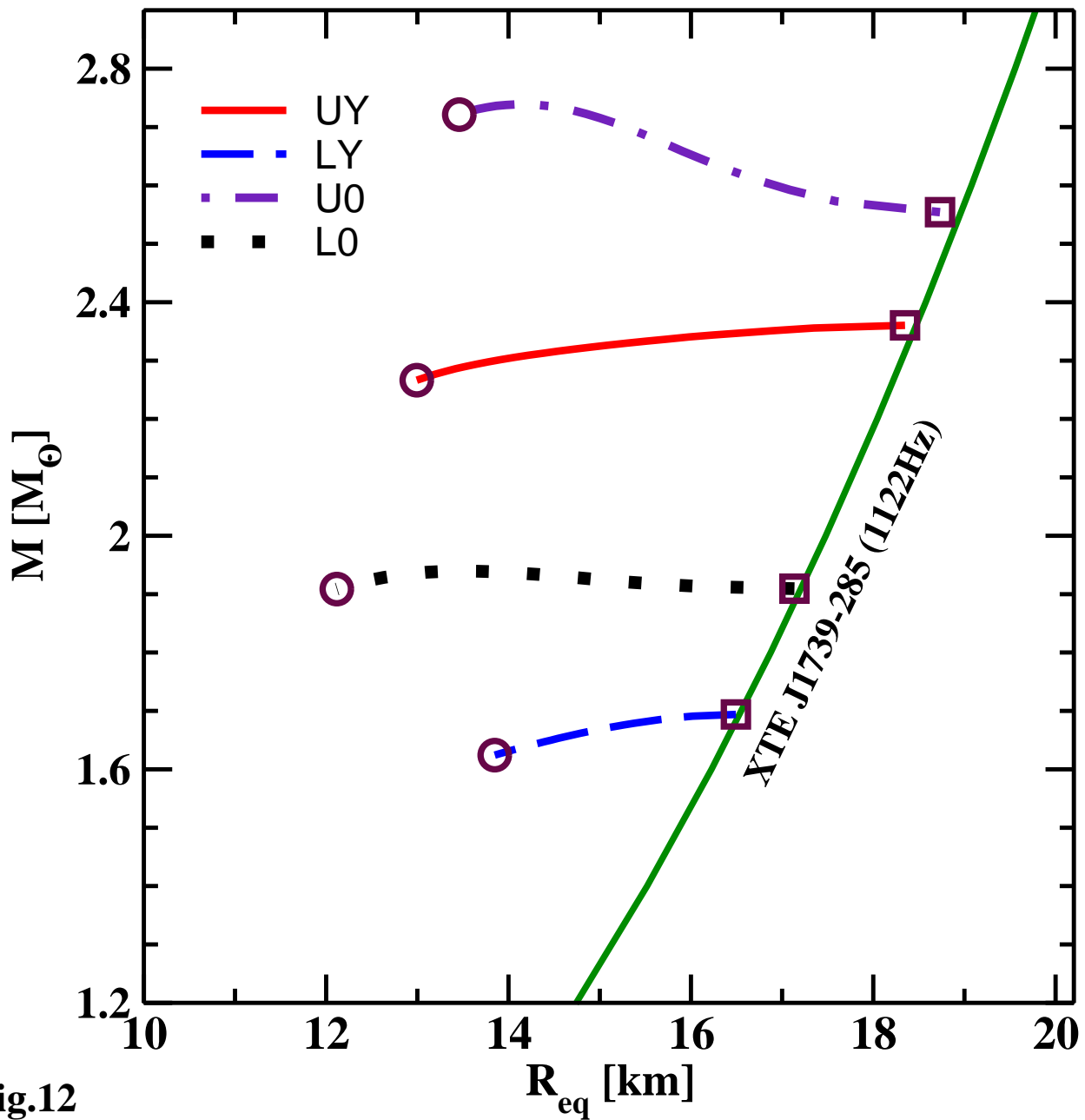


Fig.12